Master Thesis

in Geoecology,

University of Bayreuth

Elevation-dependent surface temperature changes in the Andes

Innsbruck, 9th of August 2022

Marie Charlotte Stöckhardt

Supervised by

Prof. Dr. Fabien Maussion

Prof. Dr. Christoph Thomas

Prof. Dr. Georg Wohlfahrt

Details Author:
Marie Charlotte Stöckhardt, BSc, Student M.Sc. Geoecology, University of Bayreuth
Matriculation number: 140 1242
Email: s2mestoe@uni-bayreuth.de

Details Supervisors:
Prof. Dr. Fabien Maussion, Department of Atmospheric and Cryospheric Sciences, Ice and Climate group, University of Innsbruck

Prof. Dr. Christoph Thomas, Department of Biology, Chemistry & Earth Sciences, Micrometeorology group, University of Bayreuth

Prof. Dr. Georg Wohlfahrt, Department of Ecology, Biometeorology group, University of Innsbruck

Reviewers:
Prof. Dr. Christoph Thomas
Prof. Dr. Georg Wohlfahrt

Cover Picture:
https://agroclim-huaraz.info/img/bg-home.jpg; credit: Wolfgang Gurgiser

Abstract

Surface temperatures are rising globally, but the pace of warming varies with regional factors. Recent studies reported increased rates of temperature increase with elevation, a phenomenon referred to as elevation-dependent warming (EDW). Among others, drivers of EDW include albedo changes due to an upward migration of snow- and treelines, as well as a rise of the condensation level and water vapour changes. Amplified warming in high altitudes can have a great impact on the cryosphere with consequences for downstream water availability and on mountain ecosystems, which are particularly vulnerable and sensitive to changes of climate variables. While various studies have reported the presence of EDW, it is still unclear whether the phenomenon occurs in all mountain ranges or at all elevations and what the main physical drivers are and how they vary spatially.

Especially in the Andes, EDW has not been widely studied. Due to their latitudinal and altitudinal extent, which covers a wide range of regions with different land cover and climate, they are especially interesting for understanding the phenomenon and its drivers and spatial variations. Research on EDW is impeded by many studies focusing on observations from weather stations which have limited spatial representativity. Due to complex terrain and high elevations, they are particularly sparse in many mountain ranges of the world. By exploiting satellite earth observation data, these limitations of accessibility can be overcome and analysis on the scale of whole mountain ranges and for longer time periods can be performed. In this study, I used 20 years of land surface temperature (LST) observations from the Moderate Resolution Imaging Spectroradiometers (MODIS) on board of the TERRA satellite to investigate EDW in the Andes.

I found warming to occur predominantly in the subtropics and the midlatitudes, while in the tropical Andes both, cooling and warming patterns occurred. The patterns of EDW also varied clearly with latitude with decreasing trends with elevation in the tropics while in extratropical latitudes trends increased with elevation. Results differed between day and nighttime, with daytime results showing more pronounced patterns of elevation-dependent LST trend changes. Similar results were found for the western and eastern watershed of the Andes despite climatic differences with strong gradients in humidity between the mountain sides.

Zusammenfassung

Während Temperaturen im globalen Durchschnitt ansteigen, variiert das Tempo der Erwärmung regional. Es wurde beobachtet, dass Temperaturveränderungen von Höhengradienten in Gebirgen beeinflusst werden, mit zunehmendem Temperaturanstieg in zunehmender Höhe. Verschiedene physikalische Mechanismen und Feedbacks, wie z.B. Veränderungen der Albedo durch eine Verschiebung der Schnee- und Baumgrenze in höhere Lagen und einen Anstieg des Kondensationsniveaus und der damit verbundenen Freigabe latenter Wärme, können zu höhenabhängigen Temperaturveränderungen führen.

Besonders starke Erwärmung in hohen Lagen kann u.a. besonders anfällige, auf die Klimabedingungen der Gebirgslagen angepasste Ökosysteme negativ beeinflussen und hat große Auswirkungen auf die Kryosphäre, und die damit verbundene Wasserverfügbarkeit.

Während Muster höhenabhängiger Temperaturveränderungen in verschiedenen Studien beobachtet wurden, ist noch ungeklärt, ob dieses in allen Gebirgszügen und über alle Höhenlagen vorkommt, sowie welche die wichtigsten physikalischen Faktoren dahinter sind und wie diese räumlich variieren. Vor allem in den Anden ist das Phänomen noch nicht umfassend untersucht worden. Durch die lange Nord-Süd Erstreckung und große Höhe des Gebirges ist ein breites Spektrum von Klimazonen und sozioökonomischen Zonen abgedeckt. Die Anden sind dadurch besonders geeignet um ein besseres Verständnis der räumlichen Unterschiede des höhenabhängigen Phänomens und der physikalischen Faktoren, die es antreiben, zu erlangen.

Die Erforschung der höhenabhängigen Temperaturveränderungen wird bei Studien in denen Daten von Wetterstationen verwendet werden durch eine begrenzte räumliche Abdeckung der Gebirgsregionen der Welt mit Stationen erschwert. Durch die Nutzung von Satellitendaten können diese Einschränkungen überwunden und Analysen auf der Ebene ganzer Gebirgszüge und über längere Zeiträume durchgeführt werden. In dieser Arbeit wurden Oberflächentemperatur Daten vom MODIS Sensor (Moderate Resolution Imaging Spectroradiometer), welcher sich auf dem TERRA-Satelliten befindet, über einen Zeitraum von 20 Jahren verwendet, um die Höhenabhängigkeit von Temperaturveränderungen in den Anden zu untersuchen.

Es wurden steigende Temperaturen in den Subtropen und gemäßigten Breiten beobachtet, während in den tropischen Anden sowohl Erwärmung als auch Abkühlung auftrat. Auch die Muster der Höhenabhängigkeit dieser Trends änderten sich deutlich mit dem Breitengrad mit in steigender Höhe abnehmenden Trends in den Tropen und zunehmenden Trends außerhalb der Tropen. Die Ergebnisse unterschieden sich

zwischen Tag und Nacht, wobei die Muster der Höhenabhängigkeit tagsüber ausgeprägter waren. Für die westliche und östliche Seite der Wasserscheide der Anden wurden trotz Gradienten in Niederschlagsmenge und Wasserverfügbarkeit ähnliche Ergebnisse gefunden.

Table of Contents

List of Figures

List of Tables

List of Abbreviations

DEM	Digital Elevation Model
EDW	Elevation-Dependent Warming
ET	Evapotranspiration
LST	Land Surface Temperature
LC	Land Cover
MODIS	Moderate Resolution Imaging Spectroradiometer
TOA	top-of-atmosphere

1 Introduction

1.1 Motivation and Study Objective

While climate change occurs globally, its regional manifestations vary around the world. Feedback mechanisms, short-lived forcing agents and changes of surface properties through land-use and changes in vegetation cover affect temperature changes. These temperature changes are represented by an alteration of the radiation budget stating how much energy is available at the earth's surface and by variation in the magnitudes of the terms in the surface energy balance describing the redistribution of the available energy at the earth's surface (Zeng et al. 2015). While on global average temperatures are rising, the pace of warming varies with regional factors with some areas showing cooling trends (Tudoroiu et al. 2016).

Next to several factors like e.g. latitude, elevation can play a role for regional variations in temperature trends (Myers-Smith et al. 2020; Pepin et al. 2015). Numerous studies found increasing warming rates with increasing elevation as reviewed in Pepin et al. (2015) and Pepin et al. (2022). This phenomenon is called elevation-dependent warming (EDW). It is driven by several physical mechanisms like e.g. albedo feedbacks connected to aerosol deposition and to an upward migration of the snow- and tree-line, non-linearity effects of longwave radiation and radiative effects of clouds and aerosols (Pepin et al. 2015).

Alteration of vegetation by increased warming in high altitudes influences mountainous ecosystems, which are especially fragile and likely severely affected by changing climate (La Sorte and Jetz 2010; Pepin et al. 2015). Further, the hydrological cycle is expected to change with EDW, as e.g., the high-altitude cryosphere system is altered with potentially detrimental impacts on downstream water availability (Motschmann et al. 2020).

While EDW has been observed in regional studies, it is not yet fully understood. The physical processes and driving factors behind it and whether it is a global phenomenon occurring across all mountain ranges are questions of ongoing research (Pepin et al. 2015; Krishnaswamy et al. 2014).

In this study, I will analyse EDW in the Andes, which are a less represented mountain range among the mountains of the worlds in regard of research on EDW (Toledo et al. 2021). The Andes are ideal to study the variation of EDW with climate, as they cover the tropics, subtropics and temperate zones with their 7500 km long latitudinal extent and show spatial gradients in precipitation amounts (Garreaud 2009).

As surface stations can't cover whole mountain ranges, especially as some regions are hardly accessible in mountainous terrain, research on EDW with surface weather stations is limited. With satellite data in contrary, data covering all areas in a regular grid can be obtained and can thus overcome the limitations of data coverage in mountain ranges (Tai et al. 2020; Pepin et al. 2019a). In this study, the phenomenon of EDW was studied for the time period from 2001 to 2021 in the Andes. Data of land surface temperature (LST) and land cover (LC) from Moderate Resolution Imaging Spectroradiometers (MODIS) on board of NASA's terra and aqua satellites was used.

1.2 Theory of Radiation and Surface Energy Balance

Regional manifestations of changing climate depend on parameters which alter the radiation budget and the surface energy balance (Friedl 2002; Fritschen and Simpson 1989; Kiehl and Trenberth 1997; Foken 2016):

$$-R_n = -(K\downarrow + K\uparrow + I\downarrow + I\uparrow) = H + \lambda E + G \quad (1)$$

Based on the principle of energy conservation, the sum of the sensible heat flux (H), latent heat flux (λE) and soil heat flux (G) equals the net radiation (R_n). Per definition, positive terms are going towards the earth's surface and negative terms away from it (Friedl 2002). Sensible and latent heat flux are turbulent transport processes between the surface and the atmosphere, while the soil heat flux is a molecular transport term and is thus considerably smaller in magnitude (Green et al. 2022). Net radiation is the sum of all shortwave and longwave radiative components that go towards the surface and that are reflected or emitted from the surface (Foken 2016). K↓ and I↓ are the imcoming shortwave and longwave components of solar radiation and K↑ and I↑ the equivalent outgoing radiation terms. When changes in the surface energy balance occur preferentially along an elevational gradient or at critical elevation levels, this leads to elevation-dependent warming or cooling.

Net radiation is altered if the individual radiation components change. This occurs e.g. if the surface albedo changes, which describes the ratio between incoming and outgoing shortwave radiation:

$$\alpha = -\frac{K\uparrow}{K\downarrow} \quad (2)$$

with α being the albedo. This fraction depends on properties of the surface. Surfaces which absorb more and thus reflect less shortwave radiation are darker and have a lower albedo than surfaces absorbing less shortwave radiation which appear bright (Stephens et al. 2015). Thus, elevation-dependent albedo changes occur in relation to elevation-dependent land cover changes. One case of this is the snowline retreating to higher elevations as a consequence of global warming. At the elevation, below the new snow line, where melting occurred, surface albedo is reduced, and thus a higher fraction of the incoming shortwave radiation is absorbed, leading to warming at this elevation (Figure 1). A shortening of the snow-cover duration and a change of the snow/rain ratio is also expected to be elevation-dependent and to affect temperature trends via albedo change. This can also lead to seasonal variations of EDW. The snow-albedo effect is regarded as one of the most important drivers of EDW (Pepin et al. 2015; Guo et al. 2016). Similar to the snowline migration, with rising temperatures, vegetation density can increase in higher elevated regions where temperature is likely the limiting factor to plant growth and where warming thus can lead to an upward shift of vegetation and the treeline (Li et al. 2016; Tai et al. 2020). With albedo generally being lower for forests than for other vegetation LC types like e.g. grassland, tree line rise is also expected to lead to preferential warming in the corresponding elevation (Pepin et al. 2015). Both, snow and tree line migration, are positive feedback mechanisms, as warmer temperatures resulting from the albedo changes further increase vegetation growth and snow melt rates (Russell et al. 2017). A third elevation-dependent albedo feedback occurs, with aerosol deposition on bright surfaces, like glaciers and snow-covered regions. This reduces albedo, leading to rising surface temperatures with a higher fraction of absorbed shortwave radiation which again, as positive feedback, enhances melting processes. With snow cover and glaciers being more abundant at higher elevations, the effect supports EDW (Figure 1, Ramanathan and Carmichael 2008).

The longwave radiation terms in the radiation budget depend on specific humidity and on the surface temperature. With increasing specific humidity, incoming longwave radiation increases (Pepin et al. 2015). Outgoing longwave radiation is related to temperature given by the Stephan-Boltzmann law:

$$I\uparrow = \sigma T^4 \quad (3)$$

with σ being the Stefan-Boltzmann constant, and T the surface temperature (Blevin and Brown 1971). In contrary to air temperature, which is commonly measured by a sensor in contact to the surrounding air at 1.5 m to 2 m height from the surface, surface

temperature, LST or skin temperature refers to the energy at the surface. This results from the term of net radiation, and on how this energy is distributed between the turbulent and molecular transport fluxes and influence the outgoing longwave radiation as stated in the Stephan-Boltzmann law with an LST increase leading to an increase of outgoing longwave radiation. LST and air temperature are coupled, but can differ, especially for LC changes, with LST being more sensitive to changes in vegetation cover than air temperatures (Mildrexler et al. 2011).

The relations of the longwave radiation terms to surface temperatures and to humidity can enhance EDW, as both relations are non-linear. Outgoing longwave radiation depends on the surface temperature to the power of four and thus changes for low temperatures have a bigger effect than changes for high temperatures. Similarly, below a certain threshold of specific humidity, small changes in humidity have a stronger effect on downward longwave radiation due to optical under-saturation in the longwave water vapour absorption lines. This non-linearity can also contribute to EDW, as temperatures are lower in high elevations and low values of humidity also typically occur in higher elevated regions. An increase of specific humidity and the connected non-linear increase of downward longwave radiation thus leads to preferential warming with elevation (Ruckstuhl et al. 2007; Pepin et al. 2015).

Further, clouds and aerosol particles can affect net radiation. Clouds reduce downward shortwave radiation, but increase downward longwave radiation (Kandel 1990). Aerosol particles also reduce atmospheric transmissivity and with that downward shortwave radiation at the surface (Tudoroiu et al. 2016; Kandel 1990). Thus, changes in cloud abundance and in aerosol concentration, affect surface temperatures. However, the impact on the radiation budget by changes of clouds varies regionally and research on their impacts on EDW is sparse (Kandel 1990; Moorthy et al. 2008; Pepin et al. 2015). The effects of aerosols on radiation can be elevation-dependent, as anthropogenic sources for aerosols are most abundant in lower elevations where population is denser. An increase in particles would lead to a surface dimming effect, leading to preferential cooling or decreased warming rates at lower elevations (Figure 1). A decrease on the other hand with improved air quality, can have the opposite effect (Tudoroiu et al. 2016; Pepin et al. 2015; Ramanathan and Carmichael 2008).

Besides changes of the radiation budget, a redistribution of the energy between the turbulent fluxes of the surface energy balance affects LST. Assuming a negligible effect of the molecular ground heat flux, an increase of the latent heat flux reduces the sensible heat flux and with that the LST, while a decrease of the latent heat flux correspondingly increases the sensible heat flux and leads to cooling (Green et al. 2022; Liu et al. 2016). Changes in the latent heat flux are associated with parameters like water availability,

vegetation density and species composition. An increase in evapotranspiration (ET) due to an increase of the leaf area index with vegetation changes, provided water availability not being a limiting factor results in a local reduction of LST (Li et al. 2015b). This effect of ET cooling can counteract the warming effect due to albedo reduction, as both occur in connection to changes in vegetation cover. An increase in forested area for example would result in the occurrence of both effects. According to Bonan (2008) latitude is decisive about which of the two biogeophysical mechanisms of ET changes and albedo changes predominates and governs temperature changes. It was found that tropical forests have an overall cooling effect, while boreal forests lead to warming. This is connected to forests buffering the effect of an albedo increase and connected cooling by snow in boreal forests while snow plays a minor role in tropical forests. It remains unclear which effect predominates for temperate forests (Bonan 2008). Further, related to clouds, a shift of the condensation level is a potential driver of EDW. At this level, latent heat is released, resulting in air temperature warming. With global warming and an increased dew point depression at sea level, the elevation of this level is expected to rise, resulting in EDW by shifting the area that receives warming to a higher altitude (Figure 1, Pepin et al. 2015). As air temperatures and the surface are coupled, changes in air temperatures also affect LST.

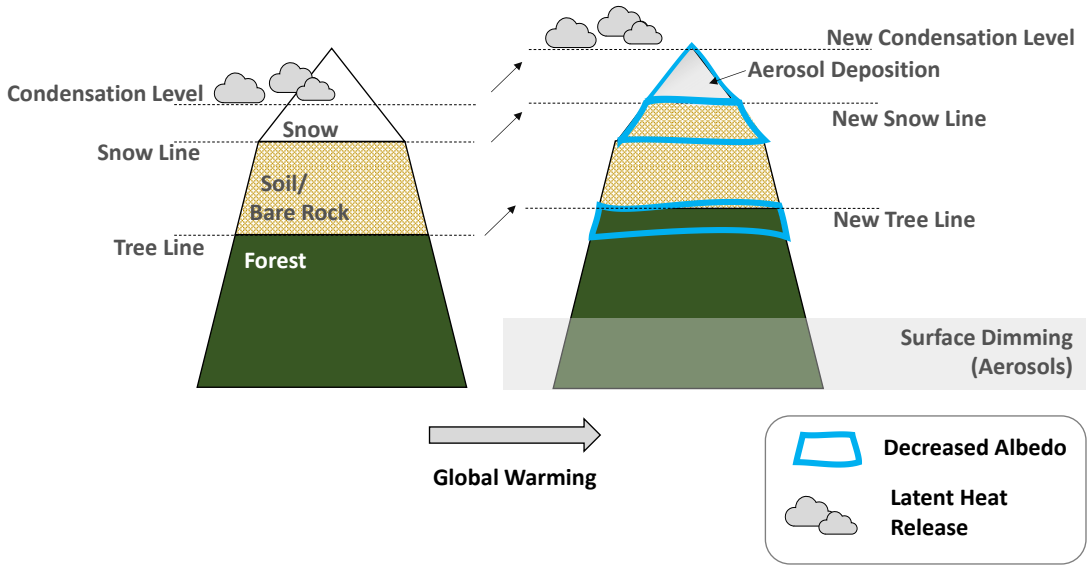

Figure 1: Schematic drawing of the driving mechanisms of EDW

1.3 Expectations and Hypotheses

The mechanisms influencing LST trends and causing EDW can vary in space and time and mostly occur simultaneously. Trends are expected to vary with LC changes, with changes from and to the LC types of forest, barren land, snow and ice in particular affecting LST trends by changing the ratio between latent and sensible heat flux and the surface albedo. LC change to forest is associated with an increase in ET rates and thus an increase in the latent heat flux which decreases the sensible heat flux and leads to cooling, while for the same change of LC albedo decreases leading to warming due to more shortwave radiation being absorbed. This counteracts on the effect of the ET increase. For changes from forest to other LC classes the opposite is expected with warming due to an ET decrease and cooling due to an albedo increase. For the overall change of LST occurring with changes from and to the LC class forest, it is decisive which of the two mechanisms prevails.

Changes from barren land are likely due to an increase in vegetation density and are thus also connected with an increase in ET rates, leading to ET cooling similarly to the LC change to forest. Albedo can either decrease or increase, depending on the surface properties of both, the barren land and the LC class to which the change occurs. Albedo can thus, either enhance the ET cooling or counteract on it in which case, like for the change to and from forest either mechanism can prevail, leading to cooling or warming. Accordingly, for changes from a LC with vegetation to barren land, ET decreases and warming is expected. Again, Albedo can either in- or decrease. For a change from and to the LC of snow and ice, the associated albedo change is expected to drive LST trends with an increase in albedo for changes to snow and ice leading to cooling, as more shortwave radiation is reflected and a decrease in albedo for a change from snow and ice to any other LC class leading to warming with more shortwave radiation being absorbed.

Major factors influencing the magnitude of EDW in the Andes, that are considered in this study, are day versus nighttime, humidity, and latitude. EDW is assumed to be observed in the whole study area, but to vary in space and time as stated in Table 1.

Due to temperature differences and as the mountain height of the Andes varies along the cordillera, latitude is expected to be a governing variable for differences in the patterns of EDW. As the area covered by snow or ice and the snow duration throughout the year increase from North to South with the zero-degree isotherm reaching lower elevations, the snow, ice and aerosol albedo feedbacks are expected to be strongest in higher latitudes (Russell et al. 2017). Tree line migration on the other hand is expected to occur across all latitudes. Whether the warming effect due to albedo decreases or the cooling effect due to an increasing latent heat flux is stronger, can depend on latitude

though, as previously discussed in chapter 1.2. Both result in elevation-dependent temperature changes, but the cooling effect of the increasing ET rates counteracts on EDW. As in tropical forests the cooling effect predominates in theory (Bonan 2008), EDW contribution of the tree line migration is expected to be weaker in the tropics than in higher latitudes. The radiation effects of clouds and aerosols and latent heat release at the condensation level are not expected to show systematic patterns along latitude. The non-linear relationship between temperature and outgoing longwave radiation is likely stronger in higher latitudes with colder climate, as the effect is strongest at lowest temperatures.

Further, the driving mechanisms of EDW can be influenced by humidity. In climate and elevations where precipitation falls at least in parts of the year as snow, the snow/ice albedo feedback is expected to be bigger for subregions with more abundant precipitation. An elevation-dependent increase in vegetation density and both, the connected redistribution of the available surface energy from the sensible to the latent heat flux inducing elevation-dependent cooling, as well as an enhancement of EDW by albedo changes with an upward migration of the tree-line, can be diminished in drier regions with water availability limiting plant growth. The effect of preferential warming around the condensation level is also likely to be stronger in more humid climate, where more clouds are formed and thus, more latent heat is released, leading to preferential warming at the level where the condensation occurs, by an increase in the sensible heat flux. In contrary, the non-linearity effect of specific humidity and outgoing longwave radiation is expected to be stronger in more arid areas, as the effect is biggest for lowest humidity contents. A systematic difference between aerosol abundance and influence on radiation along precipitation gradients on the other hand is not expected.

Regarding differences between day and nighttime, albedo effects are only apparent during daytime, because shortwave radiation is absent during the night. Additionally, effects of vegetation changes are expected to be higher at daytime with photosynthesis occurring at daytime. This leads to more pronounced changes in ET rates at daytime, which, by affecting the ration between latent and sensible heat flux, affect LST trends. Effects on the radiation budget by clouds or aerosols as well as a rise of the condensation level are not expected to systematically change with the daily cycle. The non-linearity effects of longwave radiation could shift to lower elevations at nighttime when temperatures are lower. The lower temperatures might generally enhance the effect of EDW driven by non-linearity of the longwave radiation at nighttime. Considering all of these factors, EDW should prevail during daytime.

Table 1: Overview of the expectations of where/when the relative magnitude of the main driving mechanisms on EDW in dependence of spatio-temporal aspects is strongest. '+' indicates more precipitation, '-' indicates less precipitation and 'x' indicates no systematic differences for the corresponding parameters being expected.

	Latitude	**Precipitation gradient**	**Day/ Night**
Snow/ice and aerosol albedo feedback	Higher Latitudes	+	Day
Tree albedo feedback	Higher Latitudes	+	Day
Tree-line migration and latent heat (cooling effect)	Tropical Latitudes	+	Day
Radiative effects of clouds and aerosols	x	+	x
Condensation level rise and latent heat	x	x	x
Non-linearity effects of longwave radiation	Higher Latitudes	-	Night

To gain a better understanding of spatio-temporal variations of EDW in the Andes, based on the theory of the surface energy balance and the considerations summarized in Table 1, I formulated the following hypothesis:

I There is EDW in the whole Andes for the considered study period with increasing magnitude from north to south.
II Along precipitation gradients, EDW is stronger in more humid regions.
III EDW is stronger at daytime than at nighttime.

2 Materials and Methods

2.1 Study Area: the Andes

2.1.1 Overview, Atmospheric Circulation and Climate

Reaching along South America's West coast from approximately 10 °N to 53 °S with maximum peak heights excessing 6000 m above sea level, the Andes are the southern hemisphere's most important mountain range. From North to South the Andes cover the seven countries Venezuela, Colombia, Ecuador, Peru, Bolivia, Chile and Argentina. Due to their great heights and continuity, atmospheric circulation is disrupted which leads to strongly contrasting climatic conditions on the east and western mountain side (Garreaud et al. 2009). Despite the high elevations, the average width is with 200 km quite narrow. In the subtropics, the Andes split into two mountain ranges and form the South American Altiplano, a high-level plateau, in between. Highest elevations occur in the tropical and subtropical Andes (Figure 4; Garreaud 2009).

Large scale circulation of the northern Andes is under the influence of the Hadley Cell with the equatorial trough of low pressure and the subtropical belt of high-pressure systems (Garreaud 2009). To both sides of the continent, there are oceanic anticyclones. Air masses follow the pressure gradient from the subtropical high pressure regions to the equatorial trough and, with the influence of the Coriolis force, form easterly trade winds over the northern Andes (Emck 2007). Further south, the Andes are in the zone of the Ferrel Cell with west winds arising from compensating flow between the tropical and polar regions which is deviated eastwards by the Coriolis force (Garreaud 2009).

Mid- and upper-level flows are mostly zonal with easterly flow in the tropical latitudes and west wind south of 25 °S. Low-level flow deviates from the zonal patterns of the described large-scale circulation, as the flow is mechanically blocked by the mountain chain (Figure 2). Exceptions are the northern and southern outskirts of the mountain cordillera where altitudes are lower. Roughly between 10 °S and 30 °S, the wind flows meridional from south to north on the western mountain side and north to south in the east (Espinoza et al. 2020; Garreaud 2009).

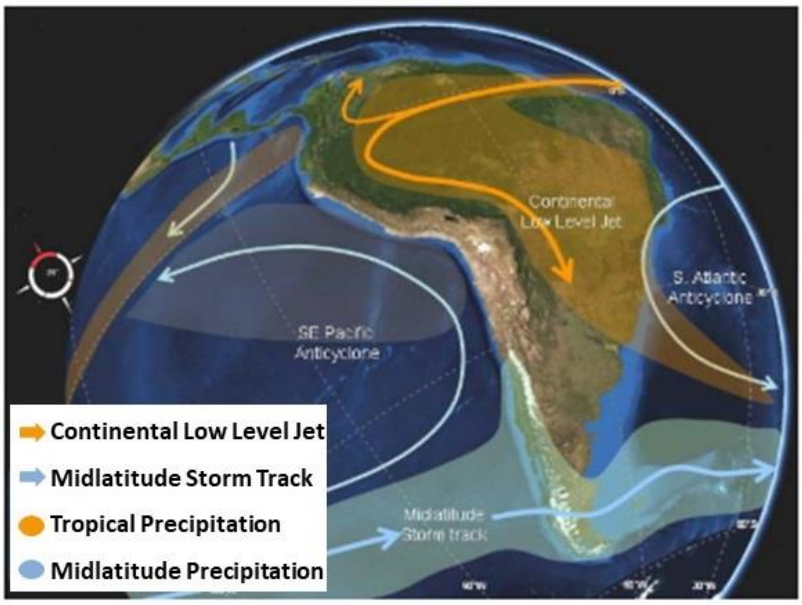

Figure 2: Schematic low-level atmospheric flow in South America (Garreaud 2009, modified)

Low-level flows are crucial for moisture transport and precipitation (Espinoza et al. 2020). The trade winds transport warm and highly moist air from the amazon region and the Atlantic Ocean to the tropical Andes. With orographic lifting, this delivers exceptional high precipitation rates to the eastern mountain side in the tropics. For some regions in Bolivia and Peru up to 6000 mm precipitation per year are reached. Accordingly, runoff amounts on the eastern mountain side in the tropics are also high. With the northern low-level flow, which is south of the trade winds, moisture from the Amazon basin is also transported to the southern tropical and northern subtropical part of the eastern Andes (Espinoza et al. 2015; Garreaud 2009; Emck 2007). Most parts on the west side of the tropical and northern subtropical Andes between 5 °S and 30 °S, on the other hand, are characterized by more arid climate. In the northern part of this area air masses descend and can, due to the connected warming, take up more moisture, leading to drier conditions. Coming from the easterly trade winds which have already lost moisture due to orographic lift effects on the eastern side. Further south, the anticyclone over the pacific supports the arid and stable conditions of the meridional low-level flow by subsiding air along the southern Peruvian and northern Chilean part of the western Andes. A cold ocean current along the coast further prevents air from taking up moisture and stabilizes the climate in this region even more, leading to exceptional arid conditions and the formation of the Atacama Desert at the western mountain side between 15 °S and 30 °S up to an elevation of 3500 m (Espinoza et al. 2020; Garreaud 2009; Houston and Hartley 2003). In the midlatitudes, similarly as in the tropics orographic effects lead to high precipitation amounts on the Luv in the west,

where the air masses are rich in moisture from the pacific. The Lee in the east is characterized by dry climate due to descending air masses (Arias et al. 2021). In the tropics, most of the precipitation falls as rain and the area that is permanently snow-covered is smallest. Snowfall only occurs at elevations approximately above 5000 m (Saavedra et al. 2018). Further south in the Andes, the 0 °C isotherm reaches down to the altitude of 500 m (Garreaud 2009). Looking at the MODIS Snow cover product for the years 2000 to 2016 and the Andes between 9 °S and 36 °S, Saavedra et al. (2018) found, that only 14 % of the total snow-covered area of the study region occurred north of 24 °S and the remaining 86 % were south of that. Thus, as summarized in Table 2, aridity varies with climate zone and mountain side with the tropical west, subtropical west and midlatitudinal east being most arid.

On an interannual scale, climate in the Andes is affected by El Niño events which has a big impact on temperature and precipitation patterns, as well as by the Pacific Decadal Oscillation and Antarctic Oscillation (Garreaud et al. 2009).

Table 2: Overview of precipitation gradients and main wind directions in the climate zones. '+' indicates more precipitation and '-' indicates less precipitation along the gradient between the mountain sides

Climate Zone	Precipitation West	Precipitation East	Main Wind Direction
Tropics	-	+	East
Subtropics	-	+	N/S
Midlatitudes	+	-	West

2.1.2 Land Surface Temperatures and Land Cover

Average annual LSTs in the study area range from -14 °C in the southern Andes to locally excessing 50 °C in the Atacama Desert in northern Chile on the western side of the mountain cordillera at daytime for average values over the study period from 2001 to 2021 (Figure 3). Lowest temperatures in the South of the Andes are expected due to the increasing latitude. The extraordinary high temperatures in the Atacama Desert are connected to the arid conditions described in section 2.1.1 and the linked absence of ET cooling. At nighttime, temperatures range from -22 °C in the southern Andes to 27 °C in the tropical Andes (Figure 3).

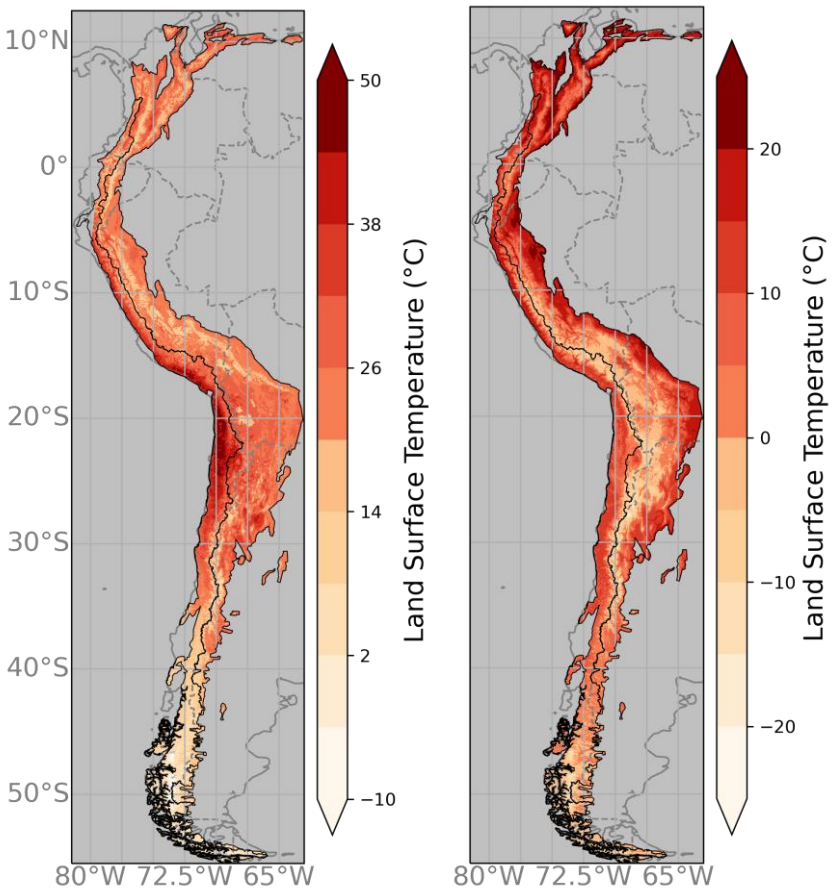

Figure 3: Average annual LST between 2001 and 2021 from MODIS Terra (MOD11A2) for daytime (left) and nighttime (right) data

The main LC classes found in the Andes by satellite data are grasslands, barren and evergreen broadleaf forests (Figure 4). Forest mostly occurs in the tropical Andes at elevations below 1500 m. South of the equator it is mostly restricted to the east side of the mountains. The majority of the western southern tropics and northern subtropics is covered by barren lands, due to the arid conditions. This is where the large Atacama

Desert is located. The tropical Andes at elevations above 1500 m are predominantly covered by grasslands. At subtropical latitudes, barren lands occur from the highest peaks to the eastern side. The lower elevations of the eastern mountain side are covered by savanna vegetation. Further south, LC mostly consists of forest, open shrubland and permanent snow and ice (Figure 4).

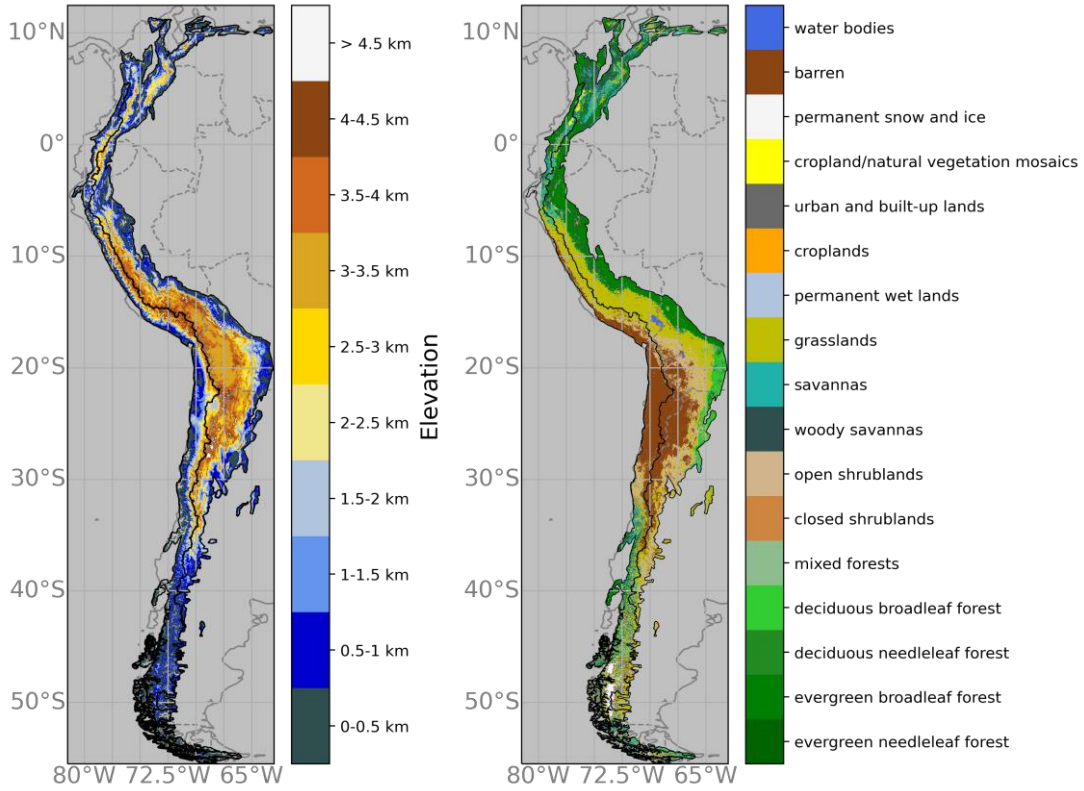

Figure 4: Topography from digital elevation model data (SRTMGL1_NC) (left) and Land Cover from MODIS (MCD12Q1) (right) in the Andes

2.2 Data Products from Remote Sensing

To investigate EDW, remotely sensed satellite data of LST, LC and a digital elevation model (DEM) were used (Table 3). The former two were measured by MODIS instruments onboard NASA's satellites Terra and Aqua. For this study, solely data from MODIS Terra were used, due to a longer period of available data starting from 2001 until the current day. For LST, according to the overfly times of the Terra satellite, passing the equator at 10:30 am and 10:30 pm each day, there are two measurements for each day. The eight-day composite product with a spatial resolution of 1 km² (MOD11A2) of these measurements were used for both, the day and the nighttime data separately. The

LC data is a combined product from both, the Terra and Aqua satellites, with a spatial resolution of 500 m and annual values (MCD12Q1). The elevation model is derived from Shuttle Radar Topography Mission data (SRTMGL1_NC). All data products were downloaded via AppEEARS (Application for Extracting and Exploring Analysis Ready Samples) from NASA's Earth Observation Data (AppEEARS Team 2022). The datasets were cut to the extent of the Andes according to the definition of which points on the earth's surface are considered as mountainous by the Global Mountain Biodiversity Assessment network for mountain biodiversity and biogeography research (Körner et al. 2017).

Table 3**:** Details on Data Products

Data Product	Spatial Resolution	Temporal Resolution	Instrument, Satellite	Reference
Land Surface Temperatures	1km	8 Days	MODIS, Terra	Wan, Z., Hook, S., Hulley, G. 2015
Land Cover Type	500m	Annual	MODIS, Terra & Aqua	Friedl, M., Sulla-Menashe, D. 2019
Digital Elevation Model	90m	Static	Synthetic Aperture Radar, Endeavour	NASA JPL 2013

2.2.1 Land Surface Temperature Product

2.2.1.1 Measurement and Preprocessing

Among other bands, MODIS sensors measure electromagnetic radiation in the thermal infrared wavelengths at top-of-atmosphere (TOA) level. Specifically, the bands 31 (10.78–11.28 μm) and 32 (11.77–12.27 μm) are used for the LST retrieval (Tomlinson et al. 2011). Based on Planck's law of the direct relation between the temperature and the emitted energy of a surface, blackbody temperatures of the surface can be calculated. To retrieve LST from TOA radiances, several corrections need to be applied, mainly to account for attenuation through the atmosphere, angular effects and spectral emissivity of the surface (Tomlinson et al. 2011). Attenuation of electromagnetic radiation occurs through absorption, reflection or refraction and scattering while passing the atmosphere with water vapor having the main influence on electromagnetic radiation in the thermal infrared wavelength (Dash et al. 2002). Angular effects arise from the different viewing angles of the satellite observations leading to shifts of the measured wavelength. Emissivity describes the amount of emitted energy from a surface in relation to the energy a blackbody would emit at the same temperature. It is highly variable and

heterogenic as it depends on parameters like land surface cover, surface moisture and roughness (Tomlinson et al. 2011; Dash et al. 2002). After applying corrections for these atmospheric effects and viewing geometry, LST can be calculated by Planck's law multiplied by spectral emissivity to account for the earth's surface emittance differing from that of a perfect blackbody:

$$R(\lambda, T) = \varepsilon(\lambda) B(\lambda, T) = \varepsilon(\lambda) \frac{c_1 \lambda^{-5}}{\pi \exp\left(\left(\frac{c_2}{\lambda T}\right) - 1\right)} \quad (4)$$

with R being the spectral radiance of a non-black body, λ the wavelength and T the temperature, $\varepsilon(\lambda)$ the spectral emissivity of a body at wavelength λ, B the spectral radiance of a black body and c_1 and c_2 universal constants (Dash et al. 2002). Ideally, Emissivity and LST should be determined simultaneously. However, by satellite measurements only, this is a mathematically under-determined problem, as the number of unknowns is larger than the number of measured parameters. Therefore, the retrieval algorithm relies on look-up tables of typical emissivity values for different land cover types (Dash et al. 2002).

The MODIS LST product MOD11A2 is preprocessed by applying a generalized split window algorithm as visualized in Figure 5 (Wan 2013; Wan and Dozier 1996). First, cloudy pixels are masked and the data for the correspondent pixels are excluded, as they refer to the cloud top reflectance instead of the attributes of the earth's surface. Second, corrections for atmospheric effects are conducted by estimations of the atmospheric column water vapor and lower boundary temperature. Corrections for the viewing geometry are integrated in viewing-angle dependent coefficients in the algorithm. Further, using an a priori knowledge of emissivity values for different land surface classes, and estimating the land-surface types of the individual pixels, band emissivities for band 31 and 32 are estimated (Wan and Dozier 1996). With that, LST values for each day and each pixel are retrieved. For the eight-day composite product, average values for each set of eight consecutive days are calculated. These averages are also conducted, if not all values within this time period exist to reduce the amount of data gaps due to cloud cover (Wan 2013). Along with the LST values, quality control flags are provided. This is based on a comparison of the results of the generalized-split-window algorithm and results from an alternative algorithm for LST conduction, the day/night LST algorithm. Additionally, factors like e.g. radiometric calibration accuracy, confidence in land-cover classification, land-cover mixture, regional topographic effects, and cirrus effects are accounted for in the quality control layer (Wan 1999). With that, information on general quality, on emissivity uncertainty and on LST uncertainty are provided for each pixel (Wan 2013).

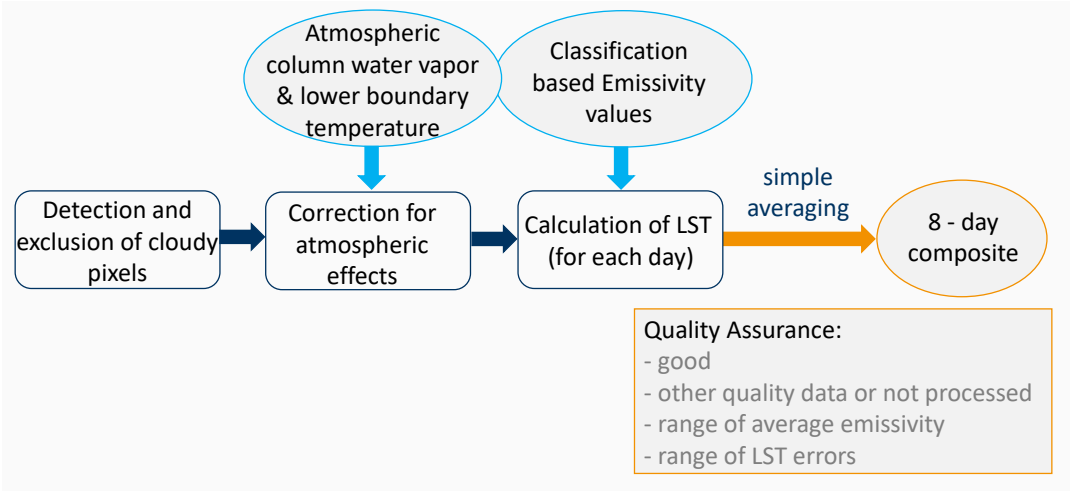

Figure 5: Preprocessing of the LST data with the generalized split window algorithm

2.2.1.2 Data Grouping and Data Availability

The dataset was spatially grouped to analyze EDW separately for regions of different climate. Along latitude, data was grouped into the climate zones tropics, north of 25 °S, subtropics between 25 °S and 37 °S and midlatitudes south of 37 °S. The latitudinal divisions at 25 °S and at 37 °S follow the definitions of the climate zones found in other studies on temperatures in the Andes (Russell et al. 2017; Zazulie et al. 2017; Toledo et al. 2021). Each climate zone was delineated into the two mountain sides. These were defined as west and east of the watershed between the Pacific and Atlantic catchment areas. This way, six subareas were generated:

- Tropics, East
- Tropics, West
- Subtropics, East
- Subtropics, West
- Midlatitudes, East
- Midlatitudes, West

To investigate elevation-dependence, the data were further grouped into elevation levels of 500 m each, shown in Figure 4, following examples from the literature (Aguilar-Lome et al. 2019; Pepin et al. 2019b). Temporally, the data product was available and treated separate for day- and nighttime values.

The total amount of pixels and their distribution in the spatial groups shows that the eastern mountain side is larger than the western side and the pixel count of the tropical domain is a larger than of the subtropics and midlatitudes, which are quite similar to each other (Figure 6). In general, pixel counts decreased along the elevation levels. Due to the occurrence of plateaus like the Altiplano the classes reaching from 3500 m to 4500 m showed a higher pixel count than elevations around this level. As pixel counts

in classes above 5000 m decreased to a negligible number, elevation levels above 4500 m were combined to a single elevation group.

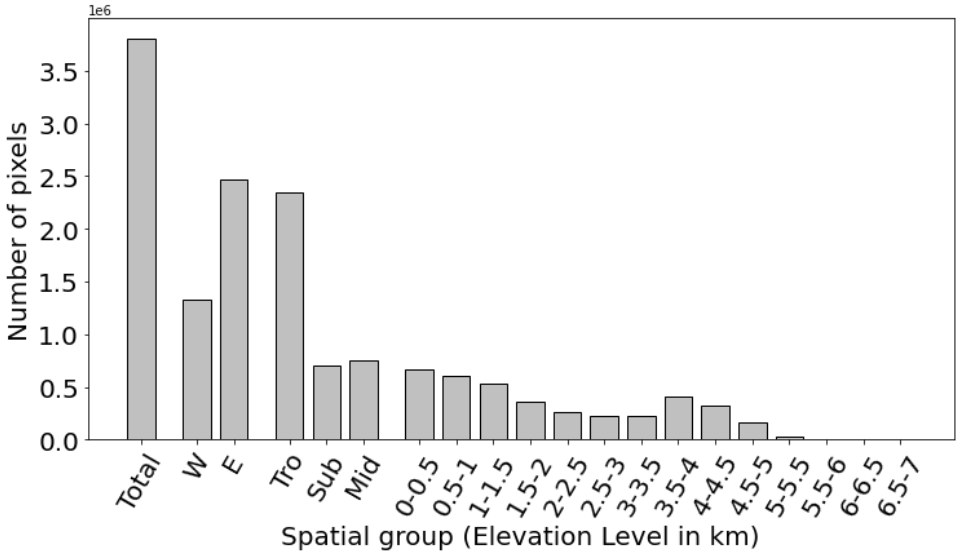

Figure 6: Pixel counts in the total area and spatial groups: mountain side, climate zone and elevation levels. W= West, E= East, Tro = Tropics, Sub = Subtropics, Mid = Midlatitudes

The data loss by the unavoidable exclusion of cloudy pixels (see section 2.2.1.1) can lead to a bias with more data loss in humid regions and in wetter seasons and can hence lead to a systematic overrepresentation of more arid regions and drier seasons. To account for spatial homogeneity of the data availability, I calculated how many values occurred in each spatial group in relation to how many values could have been measured in the spatial group in the studied time period, if there were no data gaps (Figure 7). Additionally, I compared data availability for different filter options based on the quality control layer of the LST product. The options were the categories of an average LST error smaller or equal to 1 °C, 2 °C, or 3 °C and average LST error bigger than 3 °C. For daytime data, the first two options were considered and compared to the data availability that the product has if no filter is applied. Differences in data availability between the 2 °C filter and unfiltered data were negligible small. Filtering on a maximum LST error of 1 °C in contrary reduced data availability to approximately two thirds. This would leave the group with the smallest data availability with less than 30 %. Based on that, the 2 °C filter was chosen for the analysis, similarly as other studies (e.g. Aguilar-Lome et al. 2019 and Luintel et al. 2019). Accordingly, for all performed analysis, the 2 °C filter was applied before conducting further calculations with the LST product.

For the 2 °C filtered data, data availability ranged from 60 % to nearly 100 % for the different spatial groups of climate zone, mountain side and elevation level. While no significant differences between the data availabilities at the two mountain sides were found, data availability varied between the climate zones with particularly good data availability for the subtropics due to the rare occurrence of clouds in the comparably dry subtropics. Regarding elevation, data availability increased. In contrast to the total area of the elevation levels which generally decreased with elevation (see Figure 6). In general, and specifically pronounces in the midlatitudes, data availability was higher for the nighttime than for the daytime data. Overall, data availability was at least 60 % for all spatial groups and bias by spatial heterogeneity of data availability should thus not be problematic (Figure 7).

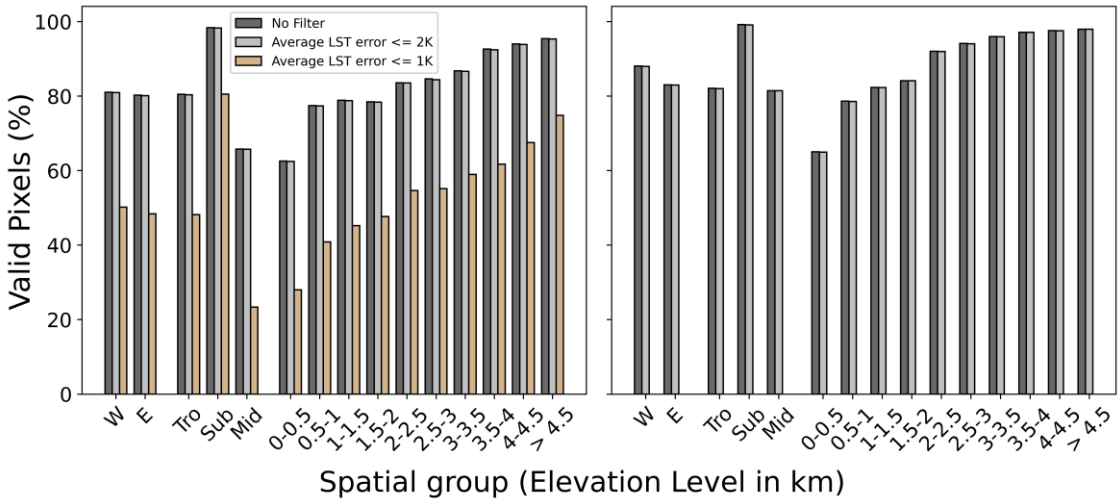

Figure 7: Data availability without filtering and with two different quality control (QC) filters applied for the spatial groups mountain side, climate zone and elevation level for daytime (left) and nighttime (right) data. Displayed are the percentages of pixels containing data in regards to the maximum possible amount of available data for the corresponding spatial group over the whole time period. W= West, E= East, Tro = Tropics, Sub = Subtropics, Mid = Midlatitudes

Temporally, data availability for each climate zone was consistent over the study period for both, day- and nighttime (Figure 8). It ranged from 40 % to 60 % for the midlatitudes at daytime to a rather stable availability close to 100 % for the subtropics at nighttime. A seasonal cycle of data availability was observed in tropical latitudes for both day and nighttime with values ranging from about 70 % to 100 %. Less pronounced, there was also a seasonality of data availability in subtropical latitudes at daytime. In the midlatitudes no obvious patterns occurred (Figure 8).

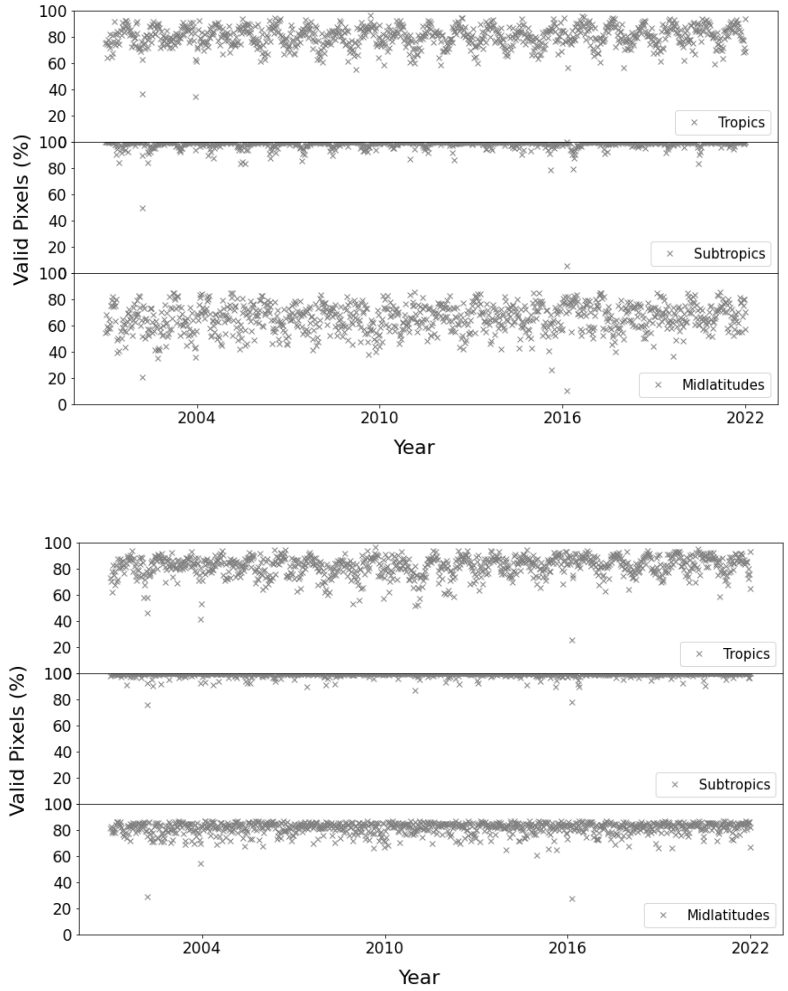

Figure 8: Data availability over time for each climate zone for daytime (top) and nighttime (bottom) data. Displayed are the percentages of pixels containing data for each point in time in regard to the maximum possible amount of available data for the corresponding climate zone.

2.2.1.3 Data Filter and Trend Calculation

Before calculating LST trends, several steps of data filtering were applied, as visualized in Figure 9. After applying the filter based on the MODIS quality control, to account for seasonal variation of data availability (Figure 8), monthly averages of the 8-day composites were calculated. Before calculating annual averages, for each pixel, I excluded all years in which more than five months were missing due to data gaps. Similarly, after calculating annual values, pixels with less than 75 % available annual averages were excluded from further analysis (Figure 9).

To test for significant trends, Mann Kendall tests for monotonic trends were performed for each pixel individually. The Mann Kendall test is a non-parametric test to assess for linear monotonic upward and downward trends over time. The null hypothesis of no monotonic trend in the dataset is tested against the alternative

hypothesis of an upward or a downward trend. The test calculates whether the difference between two consecutive data points is positive, negative or zero. With the mean and variance of these differences, Mann Kendall tests are conducted (Goswami 2017). Trend magnitudes were calculated with the Theil-Sen method (Theil 1992; Sen 1968). To identify robust trends, the resulting trends were filtered by a p-value of 0.01. Accordingly, in the following, trends with a p-value below 0.01 will be referred to as significant.

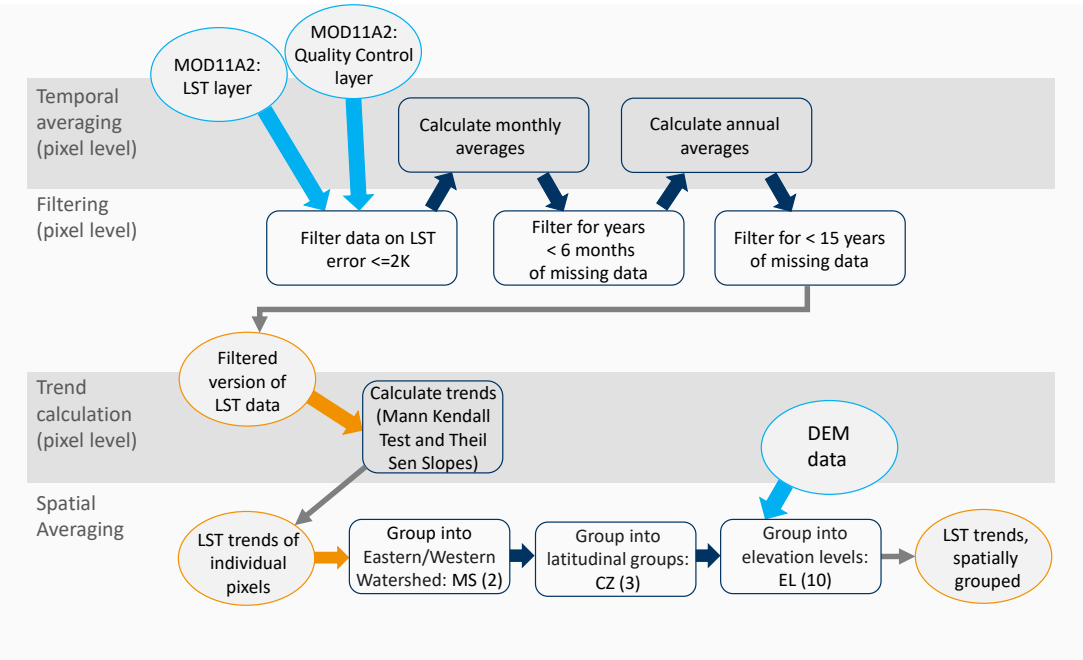

Figure 9: Schematic drawing of the filter process, trend calculation and spatial grouping of the LST product

2.2.2 Land Cover Product

To account for LC change as a driver of LST changes during the period 2001-2021, the MODIS LC product was used (Table 3). LC classification for this product was based on a supervised decision-tree classification method which used reflectance data adjusted to nadir view by a bidirectional reflectance distribution function. The classification scheme of the International Geosphere-Biosphere Programme was used (Friedl and Sulla-Menashe 2015).

In this analysis the LC change between the beginning and the end of the study period was of interest. For this, five-year windows of LC data were considered at the start (2001-2005) and the end (2017-2021) of the period. To exclude less reliable pixels with abundant LC changes, I filtered for pixels in which the LC class was consistent within

each of these five-year periods. The three LC classes evergreen broadleaf forest, permanent snow and ice and barren were selected and put in relation to daytime LST trends, as these classes are expected to particularly affect daytime LST by altering albedo and ET rates (see section 1.3).

2.2.3 Digital Elevation Model

The DEM was used for dividing LST data into elevation levels. The data product was derived from NASA's Shuttle Radar Topography Mission. Topography information was retrieved using the method of radar interferometry. For this method, with phase-coherent sensors, phase-different images are obtained from two images that are created simultaneously at slightly different locations. These images contain information on topography (Rosen et al. 2000). For this DEM, data was taken in swaths of 225 km width, and each terrain image was taken at least twice to fill areas that were shadowed by terrain by taking data from different viewing angles (Siemonsma and Dawn 2015).

3 Results and Interpretation

3.1 Annual Land Surface Temperatures

In the following, the course of annual LST over the study period was analysed with the data spatially grouped into the climate zones and mountain sides for day and for nighttime. Within each of the spatial groups for both, day and nighttime, average LST varied about 2 to 3 °C between the years (Figure 10). Spatially, the annual average LSTs follow the gradient of mountain side and climate zone as described in section 2.1 with the exception of daytime temperatures on the eastern side of the tropics being similar to the eastern side and cooler than the western side of the subtropics.

Besides latitude, humidity is expected to influence temperatures with evaporative cooling leading to lower temperatures in more humid climate. As described in section 2.1.1, the eastern tropics and subtropics and the western midlatitudes receive more precipitation than the respective other mountain side within each climate zone. In line with these considerations, daytime temperatures are approximately 7 °C to 8 °C cooler in the eastern tropics and western midlatitudes than at the corresponding more arid mountain side. In the subtropics, LSTs of both mountain sides differ by approximately 2 °C, with cooler temperatures on the more humid mountain side, as expected with more ET cooling connected to a higher water availability. Accordingly, with smaller humidity differences between subtropical west and east, the temperature differences are smaller as well. In the eastern tropics, which receive a lot of moisture from the Amazonian region, evaporative cooling is governing the lower temperatures in comparison to subtropical more arid regions like the Atacama Desert while the humid subtropics show similar temperatures.

Contrary to the daytime observations, the tropical east is the warmest and the tropical west second warmest region during nighttime. This diverging daily cycle is likely governed by radiation: at nighttime, the outgoing longwave radiation term is bigger than the incoming longwave radiation, reducing the available energy at the surface. The consequential cooling pattern is stronger pronounced for clear-sky conditions, when the term of downwelling longwave radiation is smaller, than in nights with cloudy conditions. It is thus expected to be stronger at the arid western mountain side. Further, the cooling effect of ET is usually negligible at nighttime (e.g. van Heerwaarden et al. 2010), additionally explaining smaller differences between the mountain sides during nighttime. At nighttime, the tropical east is also warmer than the subtropics. In the subtropics, the expected pattern of the eastern mountain side being colder than the west,

is also apparent. Similarly, in the midlatitudes the more humid western side is colder than the east.

Differences between day and nighttime were most pronounced in the western tropics, with an approximate amplitude of 25 °C between day and nighttime. The subtropics also have a big day night amplitude of about 20 °C, while the midlatitudes show the smallest amplitude with an average of about 10 °C. This latitudinal dependence of the magnitude of the daily cycle is expected as climate is diurnal in regions in vicinity to the equator, and seasonal further north and south towards the poles (Troll 1965).

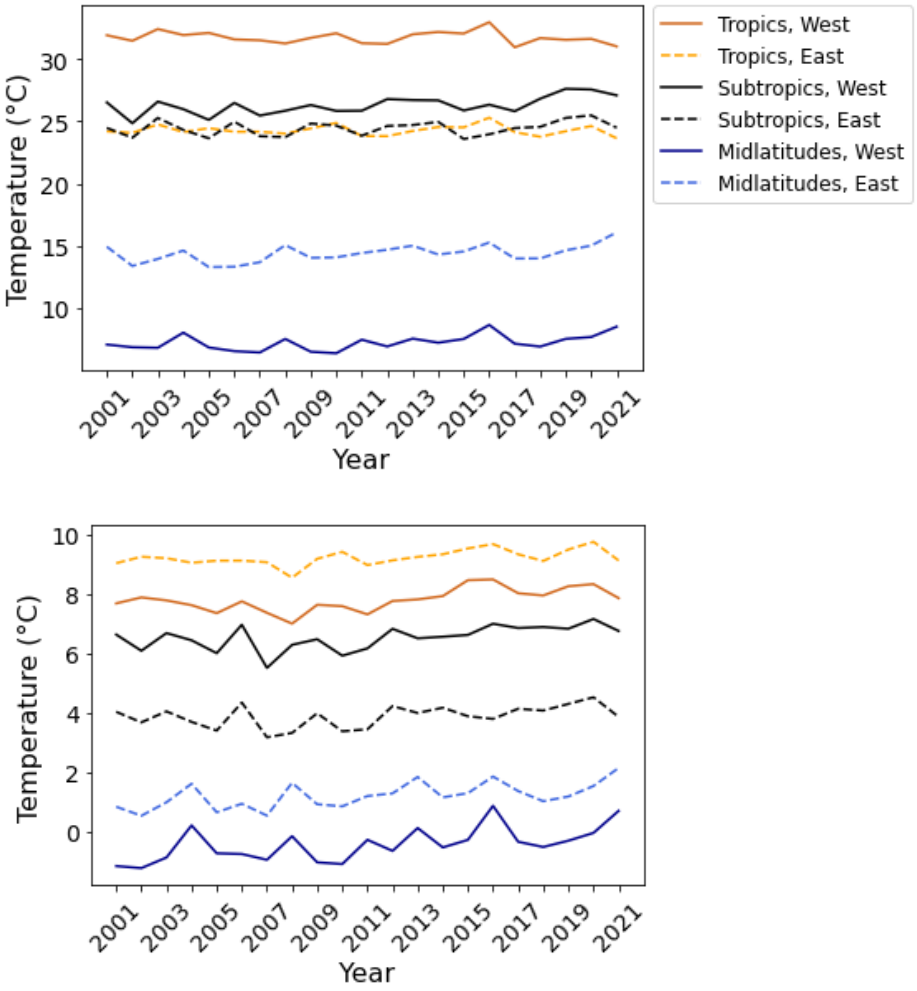

Figure 10: Time series of LST of the individual climate zones separated into the mountain sides for daytime (top) and nighttime (bottom) data.

3.2 Annual Land Surface Temperature Trends

Regarding annual trends in LST, I found more significant trends in the nighttime data than in the daytime data. Nighttime trends, however, were on average smaller in magnitude (Figure 11).

Regarding daytime data, 3.7 % of the Andes showed significant positive LST trends while 0.9 % of the mountain range were significantly negative (Figure 11). Significant warming was mostly around 1 °C per decade, but regionally reached up to around 3 °C per decade. Negative trends were mostly around minus 1 °C per decade, but also trends of minus 2 °C per decade were reached (Figure A 1). Strong and spatially consistent trends were found between 32 °S and 38 °S, i.e., in the southern subtropics and northern midlatitudes. Trend magnitudes in these regions exceeded 2 °C per decade and were higher on the eastern mountain side by approximately 0.5 °C per decade on average for this region (Figure 12). Further south of this area, for both mountain sides, warming trends were predominant, but were less abundant and with lower trend magnitudes around 1 °C per decade. Additionally, parts of the Atacama Desert in the north-western part of Chile and areas in the tropical Andes (northern outreaches and eastern Peruvian Andes) showed significant warming trends. South of the Equator, in the tropical Andes, trends differed between the mountain sides with higher trend magnitudes in the eastern Andes (Figure 11, Figure 12). Most of the negative trends occurred in the northern part of the mountain cordillera between 10 °N and 8 °S and between 8 °S to 20 °S. Further to the south little cooling spots with one noticeable patch at the western mountain side around 35°S were found.

The magnitudes of the observed trends are in a range in line with the findings of Aguilar-Lome et al. (2019) of average warming rates of 1 °C per decade in the tropical Andes for winter daytime LST of MODIS data between 2000 and 2017. Spatial variations of warming rates are expected with the mechanisms driving changes in the radiation budget and surface energy balance, as discussed in chapter 1.2. The exceptionally strong warming pattern found between 32 °S and 38 °S could be related to a reduction in snow cover, reducing albedo. Considering north-south gradients of elevation and precipitation within the Andes, the largest area that is covered by snow and by mountain glaciers is approximately at 35 °S (Zazulie et al. 2017). An upward migration of the snowline and a reduction of snow persistence throughout the year, thus affects larger areas of the land surface in this region. Amplified warming due to snow and ice albedo feedback mechanism are thus plausible to be particularly pronounced in the Andes around 35 °S. The tropical regions, where abundant daytime cooling was found, are predominantly covered by tropical forests and partly by savanna (Figure 4). Several

studies found that forests have an overall cooling effect in the tropics (Bonan 2008; Li et al. 2015b; Zeng et al. 2021). This suggests, that among the dominating biophysical effects on LST trends in forest areas the cooling effect of ET outweighs the warming effect of a low albedo (Li et al. 2015b). An increase in forest vegetation can hence be a potential reason for the observed daytime cooling.

For the nighttime data, 17.4 % of the study area showed significant positive trends and 0.5 % of the area was significantly cooling (Figure 11). The range in trend magnitude was smaller compared to daytime trends and most warming was below 1 °C per decade (Figure A 1). Compared to the daytime trends, the zonal distribution of trend magnitude had a smaller amplitude with most latitudes showing average trends between 0.5 °C and 1 °C per decade (Figure 12). A big part of the area south of 32 °S had positive nighttime trends with bigger magnitudes on the western side. In the subtropical and tropical Andes, most of the areas at the edges of the mountains were warming. Nighttime cooling mostly occurred in the northern Andes. Some local cooling patches were also found between 15 °S and 20 °S on the eastern mountain side (Figure 11, Figure 12).

While the cooling effect by ET seems to also exist in tropical forests at nighttime, it was found to be counteracted by warming by energy release of stored heat at nighttime (Li et al. 2015b). An increase in heat storage capacity at the surface by an increase in areas covered by forest vegetation and a connected increase in biomass would mean that heat stored during daytime is released at nighttime and could hence explain regional patterns in the tropics where daytime cooling and nighttime warming was found.

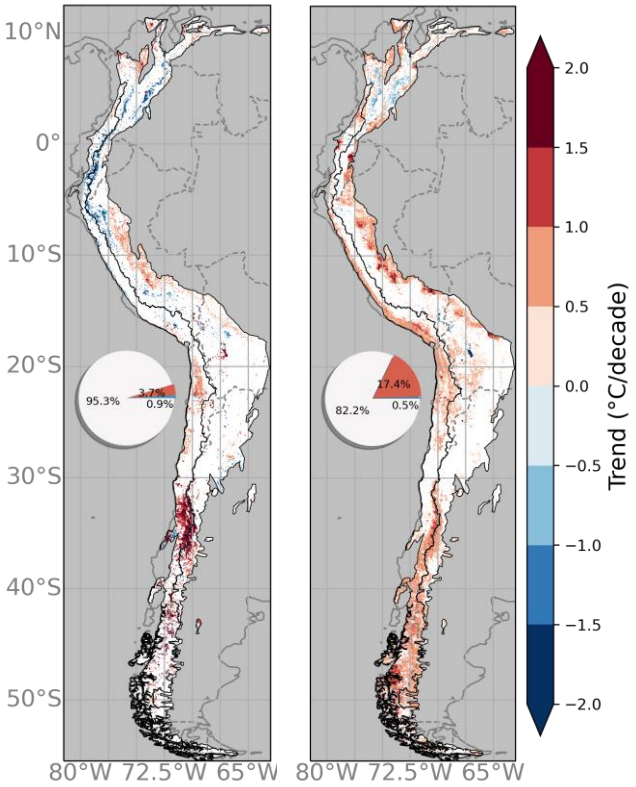

Figure 11: Annual LST trends for daytime (left) and nighttime (right) data. Only significant pixels ($p < 0.01$) are shown; white colour indicates non-significant pixels. The area of the Andes and the division between the Atlantic/Pacific watershed are indicated. Pie charts show which fractions of the trend results were positive, negative and non-significant

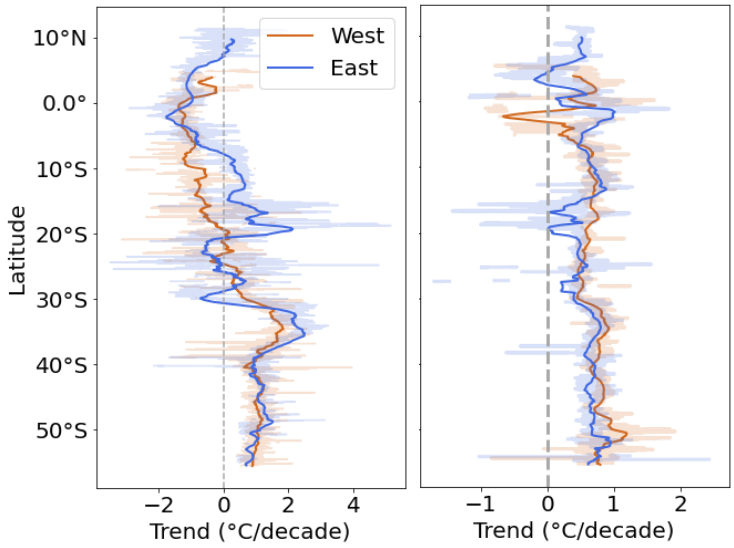

Figure 12: Zonal distribution of annual LST trends for daytime (left) and nighttime (right) data. Average trend values of significant pixels ($p < 0.01$) for each latitude are shown for both mountain sides. The bold line shows rolling zonal averages of 200 km in latitude derived from linearly interpolated zonal trend data. The background shows zonal average trend data.

3.3 Land Surface Temperature Trends and Land Cover Changes

LC transitions from and to the selected groups of evergreen broadleaf forest, snow/ice and barren land, were associated with positive average LST trends for five of the six considered cases of LC change (Figure 14). Most abundant were positive trends in the connection with LC changes from forest to any other LC type with 40% among the selected LC transitions (Figure 14). For these changes from forest, the average of the trends was 0.8 °C per decade with a standard deviation of 0.7 °C, indicating a homogeneous warming pattern. Opposed to that, the group of changes from any class to evergreen broadleaf forest, was the only group with clearly negative LST trends with an average of -1.0 °C per decade and a standard deviation of 0.8 °C (Figure 13). Hence, on average, changes to forest had a cooling effect on LST and changes from forest led to warming. This supports the explanation of the observed daytime cooling in the tropics more thoroughly described in chapter 3.2. Cooling occurs due to an increase in biomass with pixels having changed to forest vegetation leading to an increase of ET rates resulting in an overall cooling which outweighs the possible warming effect which could be attributed to a reduced surface albedo of forest LC.

Pixels changing from permanent snow or ice connected with significant LST trends were accounted for 6 % of occurring pixels among the selected transition groups. The average trend of 2.5 °C per decade for the change from snow or ice was highest among the considered groups. The positive trends for this change are in line with the expectations, as with snow and ice melting, the surface albedo decreased, resulting in warming due to more absorbed shortwave radiation. Surprisingly, LC changes from any LC class to permanent snow and ice, were associated with positive LST trends. This group was smallest with 2 % of pixels among the selected LC transitions. Here, cooling would be expected due to the albedo increase.

Similar to changes from permanent snow or ice, the transitions to barren LC were connected to greater trends with an average of 2.5 °C per decade and a standard deviation of 1.8 °C. This is likely related to removal of snow/ice surfaces and the associated albedo decrease. With LC changing from a class with vegetation to barren land, albedo can increase, which leads to cooling. At the same time, the change of the ratio between the latent and sensible heat fluxes leads to warming in this case, with a reduced latent heat flux, due to the loss of vegetation and the connected transpiration. The observed warming for the LC change to barren land indicates the warming connected to a change of the ratio of the heat fluxes to outweigh albedo cooling. The average of the trends found for pixels with changes from barren to other LC classes was also positive with 0.9 °C but had a high standard deviation of 1.7 °C ranging to negative trend magnitudes. This suggests that different patterns were combined in this group.

For pixels that change from barren to a class with more vegetation, with the related increase of ET, the surface energy balance is altered with an increase of the latent heat flux on cost of the sensible heat flux, which explains cooling trends connected to changes from barren. Depending on both the properties of the barren and the properties of the new LC class, albedo can either in- or decrease which would explain why negative as well as positive trends are observed within this group.

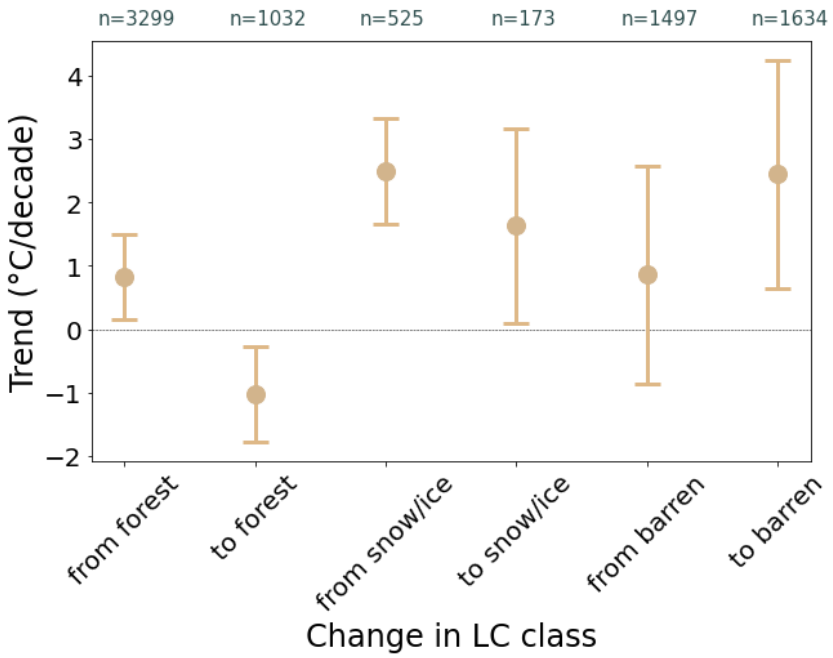

Figure 13: Significant ($p < 0.01$) daytime LST trends for pixels in which LC changes from and to selected LC classes (evergreen broadleaf forest, permanent ice and snow and barren) occurred. n gives the number of pixels in which the correspondent LC change and a significant LST trend occurred.

Most of the changes from and to evergreen broadleaf forest, permanent ice and snow and barren land occurred in the tropical Andes, north of 15 °S as well as in an area between 30 °S and 39 °S at the transition between the subtropics and the midlatitudes (Figure 14, Figure 15, Figure A 2).

In the northern Andes, changes from and to forest were the main LC changes with warming trends associated with deforestation, occurring mostly in Venezuela, the north of Columbia and Peru, and cooling trends in areas where afforestation occurred located in Columbia and Ecuador (Figure 14). This is well in line with the considerations previously mentioned in chapter 3.2 of vegetation driving daytime cooling in the tropics.

Close to the Pacific coast of Peru, there is a region where LC changed from barren land to other LC classes. These changes are connected to cooling trends. Both, higher ET rates due to more vegetation and a reduced albedo, if the new vegetation is brighter than the barren land, can lead to this cooling.

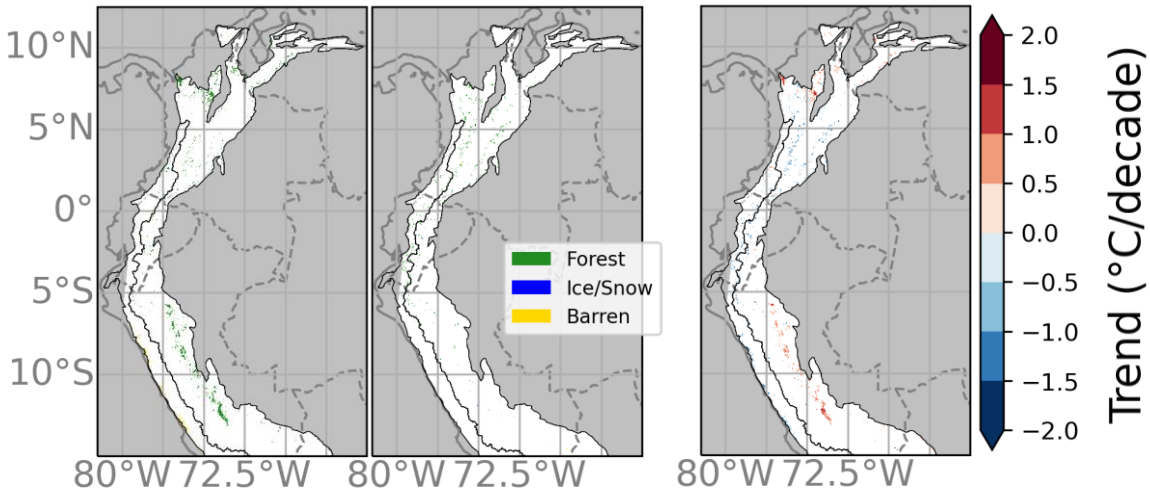

Figure 14: LC changes from selected LC classes (evergreen broadleaf forest, permanent ice and snow and barren) (left), to selected LC classes (middle) and significant ($p > 0.01$) daytime LST trends of the corresponding pixels to LC change occurrences from/to the selected groups (right) in the northern Andes

Around 35 °S in western Chile, like in the northern Andes, forest changes were associated with warming for changes from forest and cooling trends for changes to forest. This could also be driven by the effect of ET cooling.

Further, at the border between Chile and Argentina, changes from permanent ice and snow to barren occurred and were aligned with LST trends around 2 °C per decade. This supports the expectation that the strong warming in this region is connected to melting processes and the according albedo changes.

At these higher latitudes, in contrary to the patterns in Peru, changes from barren to other LC types indicate warming. In dependence of the properties of the LC class barren land changes to and of the barren land itself, albedo can either increase, leading to surface cooling, which is perhaps the mechanism observed in the tropics, or decrease, amplifying warming which seems to be the case for the area shown in Figure 15. The different effect on trends of LC changes from barren land between the tropics and the region around 35 °S explains the high standard deviation observed for this group (Figure 13).

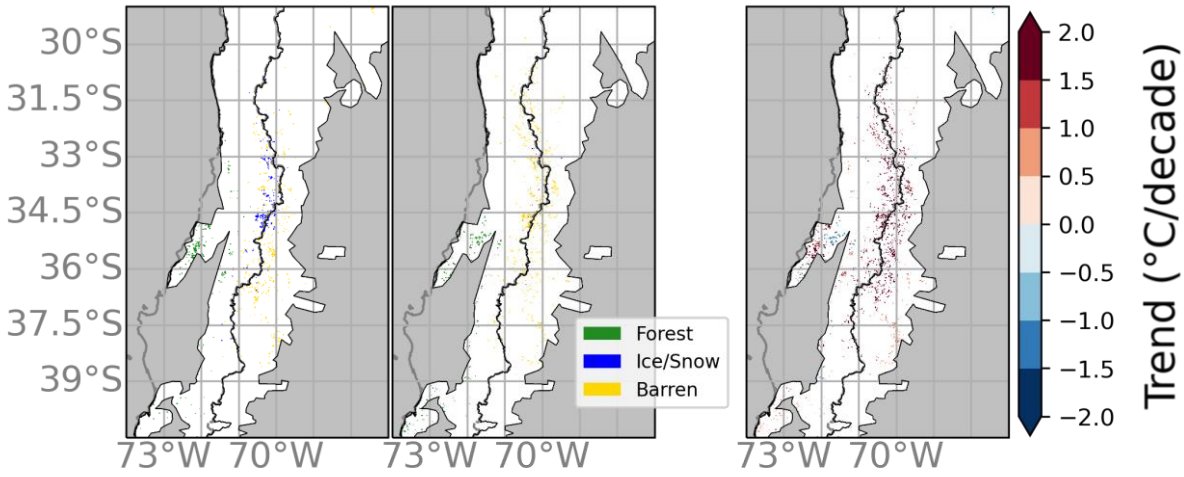

Figure 15: Same as Figure 14 but for southern Andes

3.4 Elevation-dependence of Annual Land Surface Temperature Trends

3.4.1 Overview

Elevation-dependences of LST trends were evaluated for each climate group, divided into the western and eastern side of the mountains for day and nighttime data. For the majority of the domain, average trends were positive with the exception of daytime trends in the tropics (Figure 16). Patterns of elevation-dependence differed significantly between the climate zones. For both day and nighttime the patterns were similar, but the magnitude of trend variation between the elevation levels varied significantly e.g. with an approximate range of 1.4 °C at daytime and 0.4 °C at nighttime for the western tropics as shown in Figure 16.

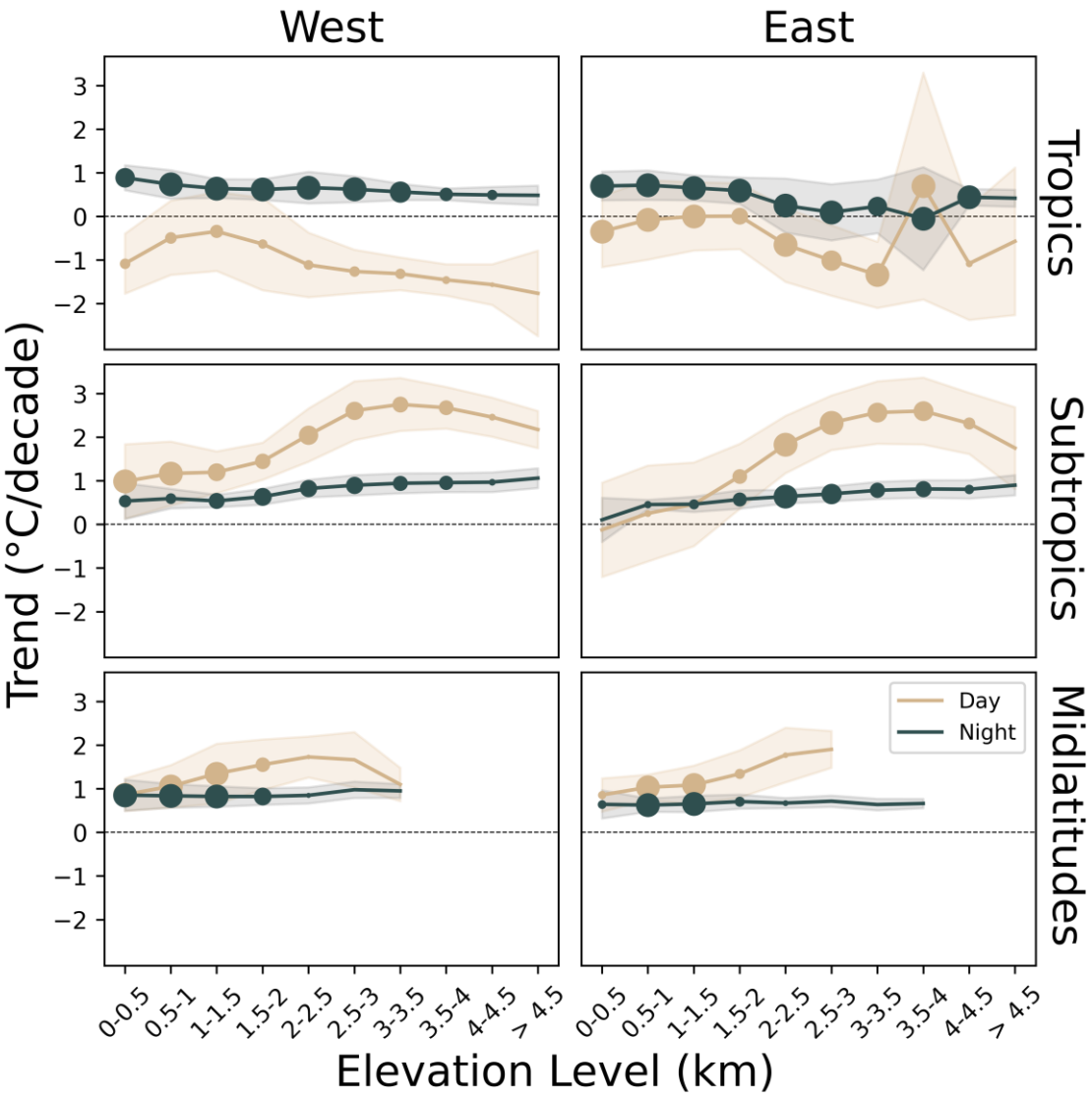

Figure 16: LST trends for each elevation level. Average values of all significant ($p < 0.01$) LST trends of the pixels in the corresponding elevation level, climate zone and mountain side are shown. The bands show the standard deviations, marker sizes indicate the number of significant trends within each group. Above 8000 significant pixels within a group, all markers have the same size, while for all groups below this threshold value, the size varies according to the number of trends in the group

3.4.2 Tropics

The averages of the tropical daytime trends were negative across all elevations for both mountain sides with the exception of the east having average trends of approximately 0 °C per decade between 1000 m and 2000 m and one elevation level (3500 m to 3400 m) in with a positive average trend of 0.7 °C per decade, but a comparably high standard deviation (Figure 16). For the lowest three elevation levels in the west and for the lowest four elevation levels in the east LST trends were decreasing

in magnitude with elevation. Above, trend magnitudes were generally increasing with elevation. For the western side, this increase in trend magnitude was from -0.3 °C per decade on average at 1000 m to 1500 m to -1.8 °C per decade. The amount of significant daytime trends for the western tropics was small for all elevations, compared to the other groups. On the eastern side, trend magnitude increased from around 0 °C per decade at 1000 m to 2000 m to a cooling of -1.3 °C per decade at 3000 m to 3500 m (Figure 16).

The decrease of daytime trends with elevation (i.e., stronger cooling in higher elevations) disagrees with the expectation of EDW as discussed in section 1.3. The abundant cooling is also surprising in the context of global warming. Supported by the analysis of LC changes to forest and the associated negative daytime LST trends in Figure 13 and Figure A 2, the daytime cooling likely occurred due to an increase in forested areas or an increase in vegetation density associated with an increase in ET rates. The elevation dependence of the negative trends could be due to an elevation dependence of the vegetation greening which leads to the observed cooling pattern along an elevation gradient as in high altitudes minimum temperatures become the limiting factor for plant growth (Tai et al. 2020). Correspondingly, the observed increase of nighttime temperatures, can lead to an upward migration of vegetation. This phenomenon, referred to as elevation-dependent vegetation greening has been observed across different studies e.g., in the Tibetean Plateau (Li et al. 2015a). Supporting the idea of vegetation changes being a driving factor for the observed daytime LST trends, Shen et al. (2015) found a negative correlation between an NDVI and maximum temperature trends over the Tibetan Plateau. Further, Toledo et al. (2021) found that albedo is not a driving mechanism on temperature trends in the tropical Andes. This supports the argument of an increase in forested area in these latitudes having led to the observed cooling via ET changes outweighing warming by albedo reduction. In contrast to my results, Toledo et al. (2021) found positive maximum temperature trends which were increasing with elevation for the tropics. A reason for different results could be the study region being restricted to the tropics south of the equator in the study of Toledo et al. (2021). The tropical regions, where I found abundant daytime cooling, which is included in the averages of my analysis on EDW, was north of this area (see Figure 11). Further, the analysed variable being air temperature and not LST, as in my study, could have led to the different results. As described in 1.2, LST is more closely linked to surface processes and stronger affected by LC changes and could thus show different trend results than air temperature. Additionally, Toledo et al. (2021) were looking at a different time period by looking at future projections, analysing air temperature differences between a period in 2071–2100 and the period 1976–2005. Vuille et al. (2015) found that the choice of the study period within the last decades played a major

role for trend results in the Andes, supporting the argument of different time periods considered explaining the deviations of my results to the literature. Similar to Toledo et al. (2021), Aguilar-Lome et al. (2019) also found daytime temperatures to be positive on average and increasing with elevation for tropical latitudes in trend calculation of MODIS LST data for the period from 2000 to 2017. Daytime cooling occurred in some pixels, spatially consistent with my results of cooling trends, but less cooling was found, than in my study. Aguilar-Lome et al. (2019) evaluated LST trends of the months June, July and August (JJA). Additional analysis of monthly daytime trends of my data revealed similar warming patterns in the study area considered by the authors for the respective months (compare Figure A 3). Including the rest of the year leads to results of more cooling than when looking only at the austral winter months. In addition, again, a different area that was included in the analysis than the region of the tropics used in my study with the northern tropics where abundant cooling occurred not being included, could explain parts of the disagreement to my results of the EDW analysis. Aguilar-Lome et al. (2019) restricted the study area to the latitudes 7 °S to 20 °S. A possible driver for the outstanding warming trends in the level from 3500 m to 4000 m on the eastern mountain side can be a rise of the condensation level and the associated increase in latent heat release.

For the nighttime data, average LST trends were positive in the tropics and ranged from approximately 0 °C to 1 °C per decade (Figure 16, a & b). In the west, trends decreased steadily with elevation from 0.9 °C to 0.5 °C per decade. In the east, trends decreased up to 3000 m, while above, no clear pattern was found. In these elevations, the standard deviation was higher than for the western side and for the lower elevations on the east (Figure 16).

The nighttime pattern of LST trends contradicts my expectations of EDW as discussed in the sections 1.2 and 1.3. In contrast to my expectations I found an inversed pattern of decreasing trends with elevation during nighttime. This is however in line with results by Toledo et al. (2021) who found decreasing temperature trends with elevation for minimum temperatures in the tropical Andes. Incoming longwave radiation was found to be the main driving factor for minimum temperatures. For the nighttime trends, change in vegetation is likely a negligible driver. Accordingly, Shen et al. (2015) found no significant correlation between NDVI and minimum temperatures. Also in line with my results, Aguilar-Lome et al. (2019) found nighttime trends to be more steady between the elevation levels. The range of their trend results is with 0.5 °C to 0.8 °C per decade consistent with my findings. They found a reduction of trend magnitude especially at the elevation level of 3500 m to 4000 m which matches the tendency in my results observed for the eastern mountain side.

3.4.3 Subtropics

In the subtropics, average LST trends showed EDW for both, day- and nighttime data (Figure 16). Daytime trends at the lowest elevation levels were 1.0 °C (-0.1 °C) per decade and rose to 2.8 °C (2.6 °C) per decade at 3000 m to 3500 m (3500 m to 4000 m) at the western (eastern) side. Above these elevation levels trends were decreasing. The increase was strongest in the elevation level from 1500 m to 3000 m in the west and from 1000 m to 3000 m in the east. Nighttime trends rose approximately linear with elevation for both mountain sides, with trends rising from 0.5 °C per decade (west) and 0.1 °C per decade (east) in the lowest elevations to about 1 °C per decade in the highest elevations on both mountain sides (Figure 16).

The positive temperature trends and EDW in the subtropics for both day and nighttime data I found, are consistent with the results of Toledo et al. (2021) and Zazulie et al. (2017). Both studies made future projections for the 21st century for the latitudes from 23 °S to 37 °S and from 30 °S to 37 °S respectively. The authors showed that parts of the observed warming trends were related to a decrease of annual snow cover. As changes in snow cover are elevation dependent, snow-albedo feedback is likely the governing driver of the EDW in these latitudes. Accordingly, Toledo et al. (2021) found Albedo changes to be a major driving factor of the subtropical EDW. Zazulie et al. (2018) found a reduction in albedo of 20 % to 60 % for the future projections until the end of the century relative to the period of 1980–2005. This reduction was projected for altitudes above 1500 m which is where I found the strongest LST trends and particularly pronounced EDW. Additionally, changes in snow cover and persistence throughout the year in the tropical and subtropical Andes from 2000 to 2016 by Saavedra et al. (2018) showed an upward migration of the snowline and decreasing snow persistence in the subtropics. Maximum change rates of snow persistence were found between 3000 m and 5000 m elevation in the subtropics, which is just above the elevation where I found strongest trends (Figure 16). This difference between elevations where I find maximum trends and Saavedra et al. (2018) found maximum snow persistence changes could be due to a higher sensitivity of LST on changes in snow persistence close to the snow line, where LC class changes to barren land occur. The same reason could apply for decreasing trends with elevation above 3000 m to 3500 m I found. Pepin et al. (2019b) also found negative EDW in the highest elevations of above 6000 m in the Himalaya. Besides changes in albedo, longwave radiation and humidity were reported as important driving factors on LST trends in the subtropics (Toledo et al. 2021).

3.4.4 Midlatitudes

Similar to the subtropics, daytime trends in the midlatitudes showed EDW for both mountain sides throughout the elevation level (Figure 16, e & f). Trends at the lowest elevation level were approximately 0.8 °C per decade and peaked 1.7 °C per decade at the elevations of 2000 m to 2500 m in the west and 2500 m to 3000 m in the east. During nighttime, the average trends were approximately 0.8 °C per decade independent of elevation (Figure 16). With that, at daytime EDW was weaker than in the subtropics and in contrary to the results of the subtropics did not occur for nighttime data.

As in the subtropics, the main driving mechanism of EDW in the midlatitudes is likely the snow-albedo feedback. The weaker EDW pattern that was observed could be due to less intense changes in snow cover. In the midlatitudes, data availability was very limited for elevation levels above 2000 m at both mountain sides implying higher uncertainties. Strongest EDW in the subtropics was observed above this elevation. This might also explain, why in contrary to the expectations of section 1.3 EDW was less pronounced in this climate zone.

3.5 Uncertainties and Limitations

Besides the discussed drivers of EDW which affect surface temperature trends by altering the radiation budget and the surface energy balance, LST trends and their distribution can also be affected by changes of regional circulation patterns and by interdecadal variability (Vuille et al. 2015; Russell et al. 2017). Vuille et al. (2015) showed that the choice of the study period within the last decades strongly affected results on LST trends and patterns of EDW. The Pacific Decadal Oscillation affects sea surface temperatures at South America's coast which in turn affect land surface temperatures in the western Andes. Congruent with this oscillation, the authors found warming between 1961 and 1990 across most of the Andes, while between 1981 and 2010 cooling was observed particularly for the tropics for coastal areas and the western slopes of the Andes. In contrast to my results, this cooling did not occur across all elevations, but in higher altitudes EDW was found (Vuille et al. 2015). Thus, interdecadal variability is likely to play a role for tropical cooling I observed, at least for regions in vicinity of the coast at the western mountain side.

Further, it should be noted that working with remotely sensed satellite data entails some unavoidable uncertainties. A major limit is the necessary exclusion of cloudy pixels with which a clear-sky bias is obtained (see also section 2.2.1). Using MODIS data, in the

Arctic, it was observed that this bias leads to an underestimation of the actual temperature with surface temperatures usually being colder at clear-sky conditions than at cloudy conditions which can be attributed to longwave radiation loss (Pepin et al. 2019a; Westermann et al. 2012). Clouds can further be a source for erroneous data, if they are not detected. In that case a strong underestimation of LST would occur, with the temperature of the cloud top being significantly colder than at the earth's surface (Westermann et al. 2012). Additionally, the calculation of LST depends on the estimation of surface spectral emissivity and hence, uncertainties connected to the determination of emissivity affect the accuracy of the retrieved LST product (Dash et al. 2002; Wan and Dozier 1996). A connected limitation occurs by heterogeneity of surface properties within the pixels of 1 km^2. A pixel of MODIS data often contains different land cover types (Wan and Dozier 1996; Pepin et al. 2019a). These can not only have different emissivity values but also different Albedo, and LSTs and the grid of pixels might be too coarse to capture small-scale differences. Mountainous terrain in particular is highly heterogeneous on small scale and this spatial heterogeneity is not depicted by the LST data product (Pepin et al. 2019a). An additional uncertainty is given by the LST error of 2 K on which I filtered the data (see section 2.2.1). As this LST error is not expected to have systematic patterns, trend results should not be affected significantly. Still, in the range of the magnitudes of the observed trends, with averages of the defined spatial groups between -2 °C and 3 °C per decade, a 2 °C uncertainty is not in a negligible magnitude. Increasing the data reliability by choosing the filter on an error of 1 °C would strongly reduce available data on the other hand (see Figure 7), which would likely lead to a spatio-temporal bias with an overrepresentation of regions and time periods of especially dry conditions, as most uncertainties result from cloud cover.

4 Conclusion

Using satellite derived LST data from MODIS from 2001 to 2021 with a spatial resolution of 1 km², several patterns of dependence of LST trends on elevation across the Andean Mountain range were revealed. I discussed EDW and its most important drivers with regard to elevation levels, along a humidity gradient between the Pacific and Atlantic watershed and the three climate zones tropics, subtropics and midlatitudes. Latitude had a strong effect on the phenomenon. The two considered times of the daily cycle at day and at night substantially affected how pronounced the observed patterns were. Climate differences in terms of humidity between the mountain sides seemed to have only minor effects on EDW. Results illustrated that EDW occurred in the subtropics and midlatitudes with stronger patterns at daytime than at nighttime. The tropics were characterized by negative daytime trends and positive nighttime trends, which both, in contrary to the patterns of the subtropics and midlatitudes decreased with increasing elevation. Additionally, I analyzed the effects of land cover change on trends in LST and showed that changes from forest and from ice/snow to another LC type as well as changes to barren land were connected to LST warming. Change from forest to other LC types was related to LST cooling.

I hypothesized that EDW occurs throughout the whole Andes for the considered time period. This was supported by the results of the extratropical zone but not by the results of the tropics. Furthermore, I hypothesized the magnitude of EDW to increase from the north to the south of the Andes. I found pronounced EDW in the subtropics, and less pronounced in the midlatitudes, while the tropics showed the opposite pattern. Accordingly, I could not confirm this part of the first hypothesis. However, I observed a strong dependence of latitude on patterns of EDW. Evaluations of LC changes suggested that gradients in snow-cover and the extent of vegetation changes drove latitudinal differences in EDW. My second hypothesis stated stronger EDW for the eastern side of the Pacific/Atlantic watershed for the tropics and subtropics and the western side for the midlatitudes due to its higher humidity. In my results, water availability did not seem to be a key driver and in general, patterns of EDW did not differ significantly between the mountain sides, not supporting the hypothesis. Finally, I expected EDW to be stronger for daytime LST than for nighttime which was supported by my results. As I identified changes in albedo as a key driver in altering the radiative terms of the surface energy balance, this day-night differences are comprehensible in respect to the lack of shortwave radiation during night. Similarly, changes in ET prominently drive changes in LST altering non-radiative components of the surface energy balance primarily at daytime.

To better understand the underlying physical processes of EDW on a large scale, future research should take a closer look at the potential driving mechanisms. This could include analysis of gridded datasets of albedo, precipitation, snow and ice cover and snow persistence. Further, variables representing vegetation variability should be included by e.g., NDVI timeseries. To disentangle EDW driven by climate change and the correspondent effects on the surface energy balance and EDW occurring due to natural interdecadal variability, data of the Pacific Decadal Oscillation could be evaluated focusing on how the oscillation correlates to LST trends. Investigating these driving factors, further insight on why the observed patterns of EDW occurred can be gained.

Acknowledgements

I would like to extent my gratitude to everyone who supported me during the work on my master thesis.

First and foremost, a special thanks goes to my supervising team, Georg, Fabien and Christoph, for making this cooperation between Bayreuth and Innsbruck possible and for always taking the time to advise and support me where you could. I was also very excited about the opportunity to present my work at the EGU. Thank you for encouraging me to participate and for supporting me during my talk in Vienna.

A big thank you to Lorenz for all your help, advice, and support. I am very grateful for your support with the coding in Python, managing the big data amounts, ideas for my graphics and advice for planning the next steps and what to focus on.

Further, I would like to thank my grandparents who have financially supported my entire master's program, allowing me to focus on the tasks and challenges of my university studies. I wish you were here with me to celebrate the achievement of my master's degree.

A special thanks to my amazing flatmates, who always cheered me up whenever the thesis was giving me a tough time, who believed in me that I could handle all the programming, writing, and presentation tasks, who took me mountain biking, on ski-tours and to the Lake Garda when they decided a break would do me good, who provided me with food and coffee, and who encouraged me to keep going and finish my work. I don't know what I would have done without you guys.

Of course, also thanks to my fellow students and friends for all the good times we spent together and for encouraging me and being there for me during all the steps of my thesis.

Finally, I would like to thank my parents and my sister for always believing in me, encouraging me and for helping and supporting me wherever they can. Thank you for always being there for me!

Appendix A: Frequency Distribution LST Trends

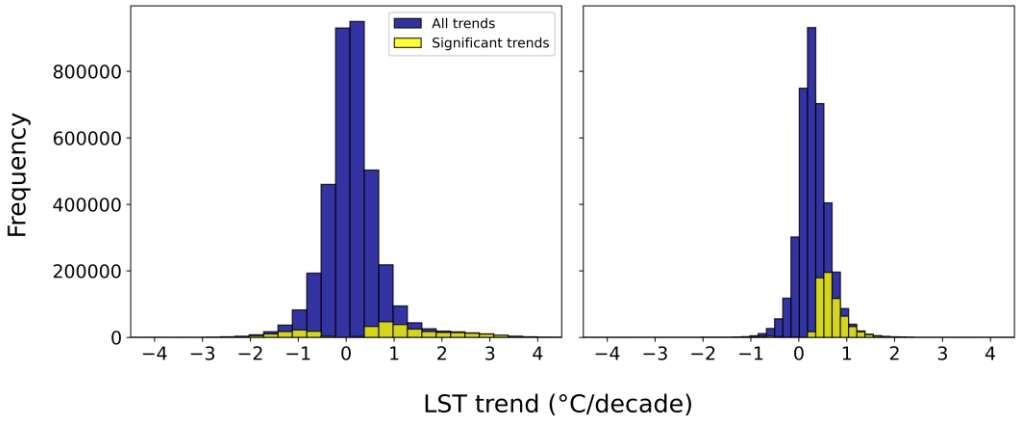

Figure A 1: Frequency distribution of LST trends in the whole study area for daytime (left) and nighttime (right) data

Appendix B: LC changes and LST trends

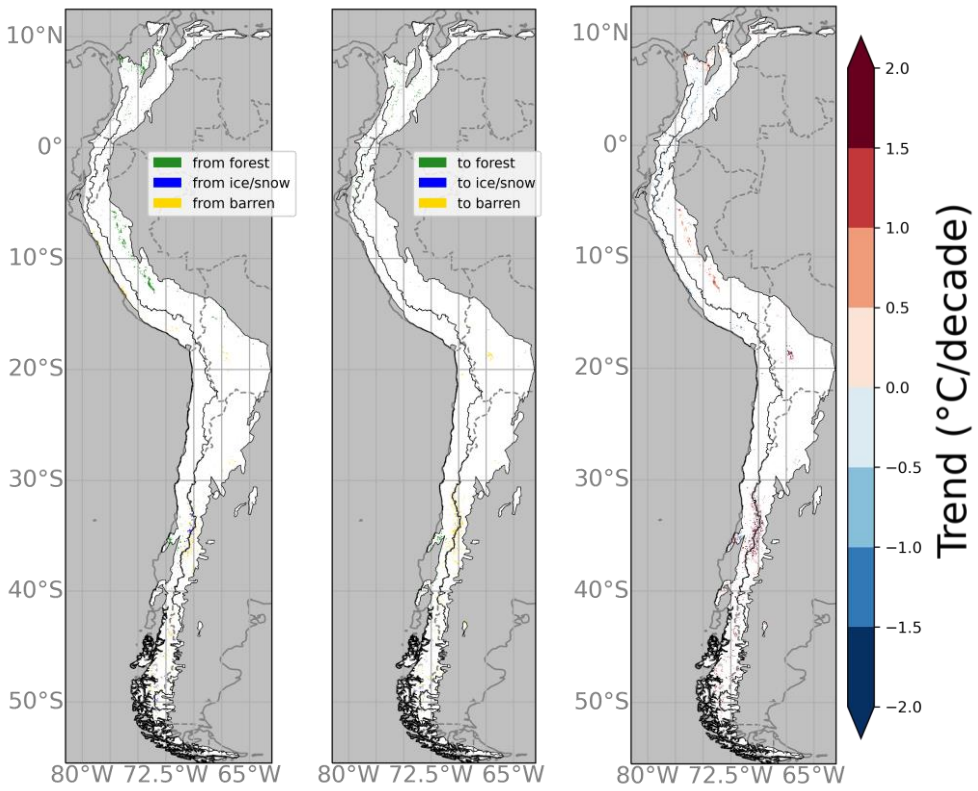

Figure A 2: LC changes from selected LC classes (evergreen broadleaf forest, permanent ice and snow and barren) (left), to selected LC classes (middle) and significant ($p > 0.01$) daytime LST trends of the corresponding pixels to LC change occurrences from/to the selected groups (right)

Appendix C: Monthly LST trends

Seasonal results of LST trends were obtained with the same methods as the annual trends (see section 2.2.1.3), but trends were calculated for monthly averages instead of annual averages.

Monthly results showed that daytime cooling in the tropics occurred throughout the whole year but was strongest in February (Figure A 3). In southern Peru and northern Bolivia, there was also a striking cooling pattern in October, which partly reversed to warming patterns in the three consecutive months. In June and partly in November cooling patterns reach further south in the subtropics. In November, also the most southern part of the Andes in the midlatitudes had negative trends. In the austral winter months (June, July, august) and in September on the other hand, for tropical latitudes south of the equator positive LST trends dominated. In the subtropics and midlatitudes warming was predominant during the whole year. Positive trends were especially strong during July, August and September for the subtropics and in October and November in the midlatitudes (Figure A 3).

At nighttime, noticeable cooling patterns in the tropics occurred as for daytime data in February and additionally in March and December (Figure A 4). In the subtropics like for daytime results, cooling was occurring in June. Further, like at daytime, cooling was apparent in the midlatitudes in September. Warming was strong in the southern tropics in January, the northern tropics in June and in the south eastern tropics as well as in the midlatitudes in October and November (Figure A 4).

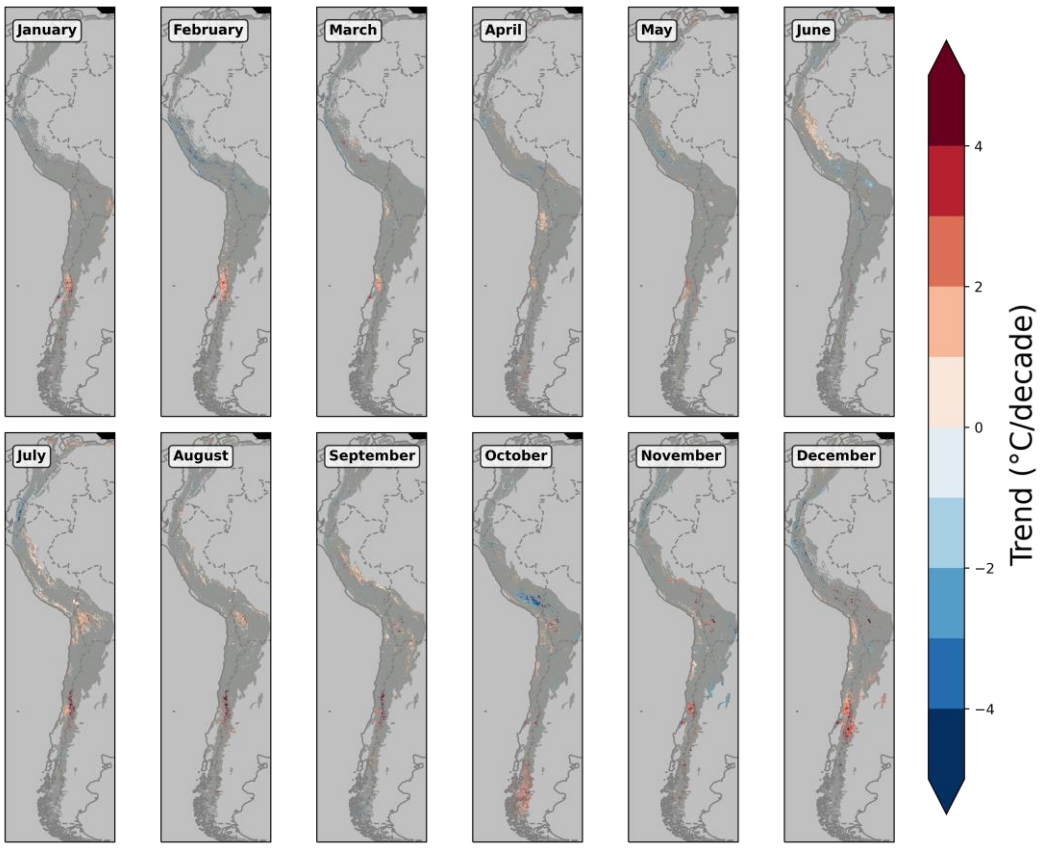

Figure A 3: Monthly LST trends for daytime data. Only significant pixels ($p < 0.01$) are shown.

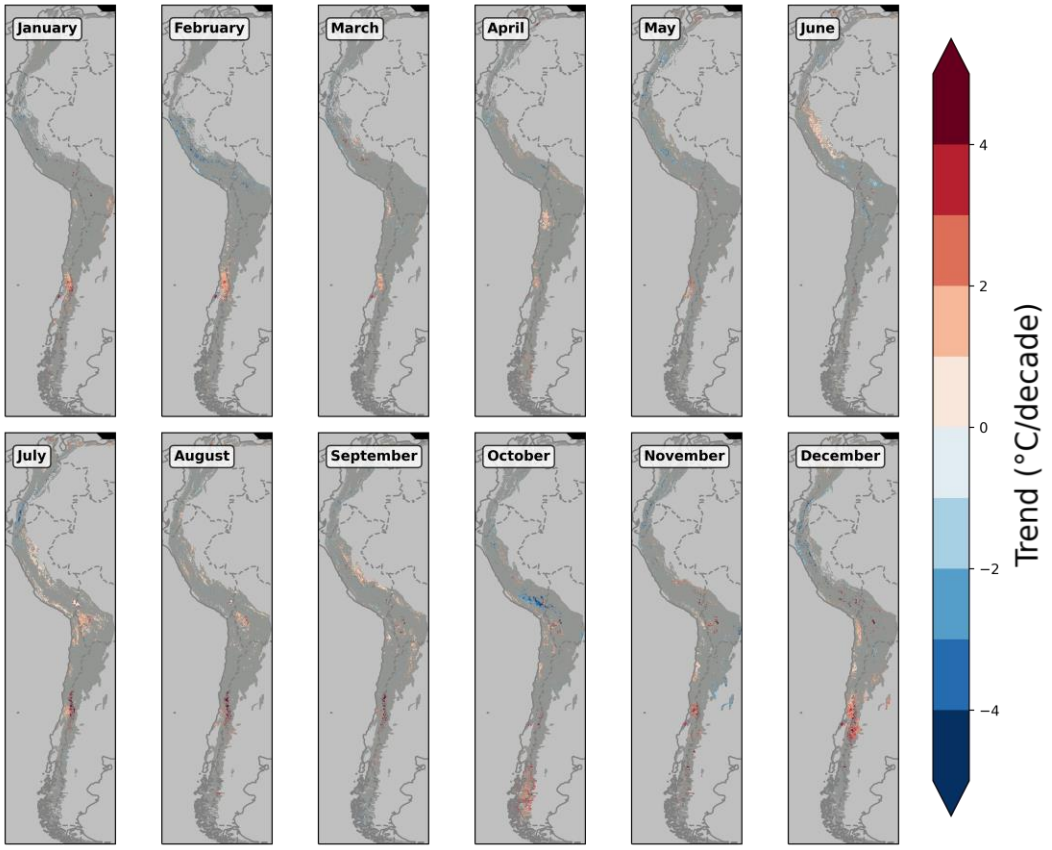

Figure A 4: Same as Figure A 3 for nighttime data

Publication bibliography

Aguilar-Lome, Jaime; Espinoza-Villar, Raúl; Espinoza, Jhan-Carlo; Rojas-Acuña, Joel; Willems, Bram Leo; Leyva-Molina, Walter-Martín (2019): Elevation-dependent warming of land surface temperatures in the Andes assessed using MODIS LST time series (2000–2017). In *International Journal of Applied Earth Observation and Geoinformation* 77, pp. 119–128. DOI: 10.1016/j.jag.2018.12.013.

AppEEARS Team (2022): Application for Extracting and Exploring Analysis Ready Samples (AppEEARS). Ver. 2.70. NASA EOSDIS Land Processes Distributed Active Archive Center (LP DAAC), USGS/Earth Resources Observation and Science (EROS) Center, Sioux Falls, South Dakota, USA. Accessed February 22, 2022. https://lpdaacsvc.cr.usgs.gov/appeears.

Arias, Paola A.; Garreaud, René; Poveda, Germán; Espinoza, Jhan Carlo; Molina-Carpio, Jorge; Masiokas, Mariano et al. (2021): Hydroclimate of the Andes Part II: Hydroclimate Variability and Sub-Continental Patterns. In *Front. Earth Sci.* 8, p. 505. DOI: 10.3389/feart.2020.505467.

Blevin, W. R.; Brown, W. J. (1971): A Precise Measurement of the Stefan-Boltzmann Constant. In *Metrologia* 7 (1), p. 15. DOI: 10.1088/0026-1394/7/1/003.

Bonan, G. B. (2008): Forests and Climate Change: Forcings, Feedbacks, and the Climate Benefits of Forests. In *Science*. DOI: 10.1126/science.1155121.

Dash, P.; Göttsche, F.-M.; Olesen, F.-S.; Fischer, H. (2002): Land surface temperature and emissivity estimation from passive sensor data: Theory and practice-current trends. In *International Journal of Remote Sensing* 23 (13), pp. 2563–2594. DOI: 10.1080/01431160110115041.

Emck, Paul (2007): A Climatology of South Ecuador - With special focus on the major Andean ridge as Atlantic-Pacific climate divide. Doctoralthesis. Friedrich-Alexander-Universität Erlangen-Nürnberg (FAU).

Espinoza, Jhan Carlo; Chavez, Steven; Ronchail, Josyane; Junquas, Clémentine; Takahashi, Ken; Lavado, Waldo (2015): Rainfall hotspots over the southern tropical Andes: Spatial distribution, rainfall intensity, and relations with large-scale atmospheric circulation. In *Water Resour. Res.* 51 (5), pp. 3459–3475. DOI: 10.1002/2014WR016273.

Espinoza, Jhan Carlo; Garreaud, René; Poveda, Germán; Arias, Paola A.; Molina-Carpio, Jorge; Masiokas, Mariano et al. (2020): Hydroclimate of the Andes Part I:

Main Climatic Features. In *Front. Earth Sci.* 8, p. 2007. DOI: 10.3389/feart.2020.00064.

Foken, Thomas (2016): Angewandte Meteorologie. Mikrometeorologische Methoden. 3rd ed. Berlin, Heidelberg: Springer Spektrum. Available online at https://link.springer.com/book/10.1007/978-3-642-25525-0.

Friedl, M. A. (2002): Forward and inverse modeling of land surface energy balance using surface temperature measurements. In *Remote Sensing of Environment* 79 (2-3), pp. 344–354. DOI: 10.1016/S0034-4257(01)00284-X.

Friedl, Mark; Sulla-Menashe, Damien (2015): MCD12C1 MODIS/Terra+Aqua Land Cover Type Yearly L3 Global 0.05Deg CMG V006.

Friedl, M., Sulla-Menashe, D. (2019): MCD12Q1 MODIS/Terra+Aqua Land Cover Type Yearly L3 Global 500m SIN Grid V006. NASA EOSDIS Land Processes DAAC. Accessed 2022-01-17 from https://doi.org/10.5067/MODIS/MCD12Q1.006. Accessed January 17, 2022.

Fritschen, Leo J.; Simpson, James R. (1989): Surface Energy and Radiation Balance Systems: General Description and Improvements. In *J. Appl. Meteor.* 28 (7), pp. 680–689. DOI: 10.1175/1520-0450(1989)028<0680:SEARBS>2.0.CO;2.

Garreaud, R. D. (2009): The Andes climate and weather. In *Adv. Geosci.* 22, pp. 3–11. DOI: 10.5194/adgeo-22-3-2009.

Garreaud, René D.; Vuille, Mathias; Compagnucci, Rosa; Marengo, José (2009): Present-day South American climate. In *Palaeogeography, Palaeoclimatology, Palaeoecology* 281 (3-4), pp. 180–195. DOI: 10.1016/j.palaeo.2007.10.032.

Goswami, B. (2017): Mann-Kendall Test (mkt). Available online at https://up-rs-esp.github.io/mkt/.

Green, Julia K.; Ballantyne, Ashley; Abramoff, Rose; Gentine, Pierre; Makowski, David; Ciais, Philippe (2022): Surface temperatures reveal the patterns of vegetation water stress and their environmental drivers across the tropical Americas. In *Global change biology* 28 (9), pp. 2940–2955. DOI: 10.1111/gcb.16139.

Guo, Donglin; Yu, Entao; Wang, Huijun (2016): Will the Tibetan Plateau warming depend on elevation in the future? In *J. Geophys. Res.* 121 (8), pp. 3969–3978. DOI: 10.1002/2016JD024871.

Houston, John; Hartley, Adrian J. (2003): The central Andean west-slope rainshadow and its potential contribution to the origin of hyper-aridity in the Atacama Desert. In *Int J Climatol* 23 (12), pp. 1453–1464. DOI: 10.1002/joc.938.

Kandel, Robert S. (1990): Satellite observation of the Earth Radiation Budget and clouds. In *Space Sci Rev* 52 (1), pp. 1–32. DOI: 10.1007/BF00704238.

Kiehl, J. T.; Trenberth, Kevin E. (1997): Earth's Annual Global Mean Energy Budget. In *Bull. Amer. Meteor. Soc.* 78 (2), pp. 197–208. DOI: 10.1175/1520-0477(1997)078<0197:EAGMEB>2.0.CO;2.

Körner, Christian; Jetz, Walter; Paulsen, Jens; Payne, Davnah; Rudmann-Maurer, Katrin; M. Spehn, Eva (2017): A global inventory of mountains for bio-geographical applications. In *Alp Botany* 127 (1), pp. 1–15. DOI: 10.1007/s00035-016-0182-6.

La Sorte, Frank A.; Jetz, Walter (2010): Projected range contractions of montane biodiversity under global warming. In *Proceedings. Biological sciences* 277 (1699), pp. 3401–3410. DOI: 10.1098/rspb.2010.0612.

Li, Haidong; Jiang, Jiang; Chen, Bin; Li, Yingkui; Xu, Yuyue; Shen, Weishou (2016): Pattern of NDVI-based vegetation greening along an altitudinal gradient in the eastern Himalayas and its response to global warming. In *Environmental monitoring and assessment* 188 (3), p. 186. DOI: 10.1007/s10661-016-5196-4.

Li, Haidong; Li, Yingkui; Shen, Weishou; Li, Yanan; Lin, Jie; Lu, Xiaoyu et al. (2015a): Elevation-Dependent Vegetation Greening of the Yarlung Zangbo River Basin in the Southern Tibetan Plateau, 1999–2013. In *Remote Sensing* 7 (12), pp. 16672–16687. DOI: 10.3390/rs71215844.

Li, Yan; Zhao, Maosheng; Motesharrei, Safa; Mu, Qiaozhen; Kalnay, Eugenia; Li, Shuangcheng (2015b): Local cooling and warming effects of forests based on satellite observations. In *Nature communications* 6, p. 6603. DOI: 10.1038/ncomms7603.

Liu, Fengshan; Tao, Fulu; Liu, Jiyuan; Zhang, Shuai; Xiao, Dengpan; Wang, Meng et al. (2016): Effects of land use/cover change on land surface energy partitioning and climate in Northeast China. In *Theor Appl Climatol* 123 (1-2), pp. 141–150. DOI: 10.1007/s00704-014-1340-7.

Luintel, Nirajan; MA, Weiqiang; Ma, Yaoming; Wang, Binbin; Subba, Sunil (2019): Spatial and temporal variation of daytime and nighttime MODIS land surface temperature across Nepal. In *Atmospheric and Oceanic Science Letters* 12 (5), pp. 305–312. DOI: 10.1080/16742834.2019.1625701.

Moorthy, K. Krishna; Satheesh, S. K.; Babu, S. Suresh; Dutt, C. B. S. (2008): Integrated Campaign for Aerosols, gases and Radiation Budget (ICARB): An overview. In *J Earth Syst Sci* 117 (1), pp. 243–262. DOI: 10.1007/s12040-008-0029-7.

Motschmann, Alina; Huggel, Christian; Carey, Mark; Moulton, Holly; Walker-Crawford, Noah; Muñoz, Randy (2020): Losses and damages connected to glacier retreat in the Cordillera Blanca, Peru. In *Climatic Change* 162 (2), pp. 837–858. DOI: 10.1007/s10584-020-02770-x.

Myers-Smith, Isla H.; Kerby, Jeffrey T.; Phoenix, Gareth K.; Bjerke, Jarle W.; Epstein, Howard E.; Assmann, Jakob J. et al. (2020): Complexity revealed in the greening of the Arctic. In *Nat. Clim. Chang.* 10 (2), pp. 106–117. DOI: 10.1038/s41558-019-0688-1.

NASA JPL (2013): NASA Shuttle Radar Topography Mission Global 3 arc second NetCDF. NASA EOSDIS Land Processes DAAC. Accessed 2021-07-03 from https://doi.org/10.5067/MEaSUREs/SRTM/SRTMGL3_NC.003. Accessed July 3, 2021.

Pepin, N. C.; Arnone, E.; Gobiet, A.; Haslinger, K.; Kotlarski, S.; Notarnicola, C. et al. (2022): Climate Changes and Their Elevational Patterns in the Mountains of the World. In *Reviews of Geophysics* 60 (1). DOI: 10.1029/2020RG000730.

Pepin, N. C.; Bradley, R. S.; Diaz, H. F.; Baraer, M.; Caceres, E. B.; Forsythe, N. et al. (2015): Elevation-dependent warming in mountain regions of the world. In *Nature Clim Change* 5 (5), pp. 424–430. DOI: 10.1038/nclimate2563.

Pepin, Nicholas C.; Pike, Gary; Read, Spencer; Williams, Ryan (2019a): The ability of moderate resolution imaging spectroradiometer land surface temperatures to simulate cold air drainage and microclimates in complex Arctic terrain. In *Int. J. Climatol* 39 (2), pp. 953–973. DOI: 10.1002/joc.5854.

Pepin, Nick; Deng, Haijun; Zhang, Hongbo; Zhang, Fan; Kang, Shichang; Yao, Tandong (2019b): An Examination of Temperature Trends at High Elevations Across the Tibetan Plateau: The Use of MODIS LST to Understand Patterns of Elevation-Dependent Warming. In *J. Geophys. Res. Atmos.* 1 (1), p. 22. DOI: 10.1029/2018JD029798.

Ramanathan, V.; Carmichael, G. (2008): Global and regional climate changes due to black carbon. In *Nature Geosci* 1 (4), pp. 221–227. DOI: 10.1038/ngeo156.

Rosen, P. A.; Hensley, S.; Joughin, I. R.; Li, F. K.; Madsen, S. N.; Rodriguez, E.; Goldstein, R. M. (2000): Synthetic aperture radar interferometry. In *Proc. IEEE* 88 (3), pp. 333–382. DOI: 10.1109/5.838084.

Ruckstuhl, Christian; Philipona, Rolf; Morland, June; Ohmura, Atsumu (2007): Observed relationship between surface specific humidity, integrated water vapor, and

longwave downward radiation at different altitudes. In *J. Geophys. Res.* 112 (D3). DOI: 10.1029/2006JD007850.

Russell, Alexandria M.; Gnanadesikan, Anand; Zaitchik, Benjamin (2017): Are the Central Andes Mountains a Warming Hot Spot? In *Journal of Climate* 30 (10), pp. 3589–3608. DOI: 10.1175/JCLI-D-16-0268.1.

Saavedra, Freddy A.; Kampf, Stephanie K.; Fassnacht, Steven R.; Sibold, Jason S. (2018): Changes in Andes snow cover from MODIS data, 2000–2016. In *The Cryosphere* 12 (3), pp. 1027–1046. DOI: 10.5194/tc-12-1027-2018.

Sen, Pranab Kumar (1968): Estimates of the Regression Coefficient Based on Kendall's Tau. In *Journal of the American Statistical Association* 63 (324), pp. 1379–1389. DOI: 10.1080/01621459.1968.10480934.

Shen, Miaogen; Piao, Shilong; Jeong, Su-Jong; Liming Zhou; Zhenzhong Zeng; Philippe Ciais et al. (2015): Evaporative cooling over the Tibetan Plateau induced by vegetation growth. In *PNAS* 112 (30), pp. 9299–9304. DOI: 10.1073/pnas.1504418112.

Siemonsma; Dawn (2015): The Shuttle Radar Topography Mission (SRTM) Collection User Guide.

Stephens, Graeme L.; O'Brien, Denis; Webster, Peter J.; Pilewski, Peter; Kato, Seiji; Li, Jui-lin (2015): The albedo of Earth. In *Reviews of Geophysics* 53 (1), pp. 141–163. DOI: 10.1002/2014RG000449.

Tai, Xiaoli; Epstein, Howard E.; Li, Bo (2020): Elevation and Climate Effects on Vegetation Greenness in an Arid Mountain-Basin System of Central Asia. In *Remote Sensing* 12 (10), p. 1665. DOI: 10.3390/rs12101665.

Theil, Henri (1992): A Rank-Invariant Method of Linear and Polynomial Regression Analysis. In Baldev Raj, Johan Koerts (Eds.): Henri Theil's Contributions to Economics and Econometrics. Econometric Theory and Methodology, vol. 23. Dordrecht: Springer-Science+Business Media (Springer eBook Collection, 23), pp. 345–381.

Toledo, Osmar; Palazzi, Elisa; Cely Toro, Iván Mauricio; Mortarini, Luca (2021): Comparison of elevation-dependent warming and its drivers in the tropical and subtropical Andes. In *Clim Dyn*. DOI: 10.1007/s00382-021-06081-4.

Tomlinson, Charlie J.; Chapman, Lee; Thornes, John E.; Baker, Christopher (2011): Remote sensing land surface temperature for meteorology and climatology: a review. In *Met. Apps* 18 (3), pp. 296–306. DOI: 10.1002/met.287.

Troll, C. (1965): Seasonal Climates of the Earth. In : Weltkarten zur Klimakunde / World Maps of Climatology: Springer, Berlin, Heidelberg, pp. 19–25. Available online at https://link.springer.com/chapter/10.1007/978-3-642-52436-3_4.

Tudoroiu, M.; Eccel, E.; Gioli, B.; Gianelle, D.; Schume, H.; Genesio, L.; Miglietta, F. (2016): Negative elevation-dependent warming trend in the Eastern Alps. In *Environ. Res. Lett.* 11 (4), p. 44021. DOI: 10.1088/1748-9326/11/4/044021.

van Heerwaarden, Chiel C.; Vilà-Guerau de Arellano, Jordi; Gounou, Amanda; Guichard, Françoise; Couvreux, Fleur (2010): Understanding the Daily Cycle of Evapotranspiration: A Method to Quantify the Influence of Forcings and Feedbacks. In *Journal of Hydrometeorology* 11 (6), pp. 1405–1422. DOI: 10.1175/2010JHM1272.1.

Vuille, Mathias; Franquist, Eric; Garreaud, René; Lavado Casimiro, Waldo Sven; Cáceres, Bolivar (2015): Impact of the global warming hiatus on Andean temperature. In *J. Geophys. Res. Atmos.* 120 (9), pp. 3745–3757. DOI: 10.1002/2015JD023126.

Wan, Z. (1999): MODIS Land-Surface TemperatureAlgorithm Theoretical Basis Document(LST ATBD).

Wan, Zhengming (2013): Collection-6 MODIS Land Surface Temperature Products Users' Guide. Santa Barbara, December 2013.

Wan, Zhengming; Dozier, J. (1996): A generalized split-window algorithm for retrieving land-surface temperature from space. In *IEEE Trans. Geosci. Remote Sensing* 34 (4), pp. 892–905. DOI: 10.1109/36.508406.

Wan, Z., Hook, S., Hulley, G. (2015): MOD11A2 MODIS/Terra Land Surface Temperature/Emissivity 8-Day L3 Global 1km SIN Grid V006. NASA EOSDIS Land Processes DAAC. Accessed 2022-01-13 from https://doi.org/10.5067/MODIS/MOD11A2.006. Accessed January 13, 2022.

Westermann, Sebastian; Langer, Moritz; Boike, Julia (2012): Systematic bias of average winter-time land surface temperatures inferred from MODIS at a site on Svalbard, Norway. In *Remote Sensing of Environment* 118, pp. 162–167. DOI: 10.1016/j.rse.2011.10.025.

Zazulie, Natalia; Rusticucci, Matilde; Raga, Graciela B. (2017): Regional climate of the subtropical central Andes using high-resolution CMIP5 models—part I: past performance (1980–2005). In *Clim Dyn* 49 (11-12), pp. 3937–3957. DOI: 10.1007/s00382-017-3560-x.

Zazulie, Natalia; Rusticucci, Matilde; Raga, Graciela B. (2018): Regional climate of the Subtropical Central Andes using high-resolution CMIP5 models. Part II: future projections for the twenty-first century. In *Clim Dyn* 51 (7-8), pp. 2913–2925. DOI: 10.1007/s00382-017-4056-4.

Zeng, Zhenzhong; Chen, Anping; Ciais, Philippe; Li, Yue; Li, Laurent Z. X.; Vautard, Robert et al. (2015): Regional air pollution brightening reverses the greenhouse gases induced warming-elevation relationship. In *Geophys. Res. Lett.* 42 (11), pp. 4563–4572. DOI: 10.1002/2015GL064410.

Zeng, Zhenzhong; Wang, Dashan; Yang, Long; Wu, Jie; Ziegler, Alan D.; Liu, Maofeng et al. (2021): Deforestation-induced warming over tropical mountain regions regulated by elevation. In *Nature Geosci* 14 (1), pp. 23–29. DOI: 10.1038/s41561-020-00666-0.

Declaration of Authorship

I herewith certify that the work presented above is to the best of my knowledge and belief original and the result of my own investigations. Third party work, non-published and published information I received are properly and duly acknowledged. This work has never previously been submitted to any other examination committee.

Innsbruck, 09.08.2022 _____

(Marie Stöckhardt)